UNIVERSITY OF BUCHAREST

FACULTY OF CHEMISTRY

DOCTORAL SCHOOL IN CHEMISTRY

PHD THESIS SUMMARY

Homometallic and Heterometallic Complexes of Compartmental and Non-Compartmental Schiff-base Ligands and their Magnetic and Luminescent Properties

PhD Student: **PhD Supervisor:**

Masood Sarwar   **Acad. Prof. Dr. Marius Andruh**

2013

UNIVERSITY OF BUCHAREST

FACULTY OF CHEMISTRY

DOCTORAL SCHOOL IN CHEMISTRY

PhD THESIS SUMMARY

Homometallic and Heterometallic Complexes of Compartmental and Non-Compartmental Schiff-base Ligands and their Magnetic and Luminescent Properties

PhD Student: PhD Supervisor:

Masood Sarwar   Acad. Prof. Dr. Marius Andruh

Doctoral Commission:

President: Prof. Dr. Camelia Bala

PhD Supervisor: **Acad. Prof. Dr. Marius Andruh**

Official Refrees:

1. Prof. Dr. Ioana Jitaru, Politechnic University, Bucharest.

2. Dr. Oana Carp, CP-I, "I. G. Murgulescu" Institute of Physical Chemistry, Romanian Academy, Bucharest.

3. Prof. Dr. Tudor Rosu, University of Bucharest.

2013

(Pages, Chapters, figures, schemes and references numbering is according to the PhD thesis)

Table of Contents

2. Chapter 2. Heterodinuclear [Zn^{II}Ln^{III}] Complexes with Luminescent Properties

4.   Chapter 4. Heterodinuclear [$Cu^{II}Ln^{III}$] Complexes with Magnetic Properties

5.   Chapter 5. Heteronuclear [$Fe^{III}Ln^{III}$] Complexes

Dissemination of Scientific Results   A33

Introduction

The goals of this PhD Thesis were the design and synthesis of new compartmental and non-compartmental Schiff-base ligands which can be used to synthesize new binuclear and polynuclear complexes exhibiting interesting magnetic and luminescence properties. The achievement of our objectives was realized by working in accordance with the principles of crystal engineering and supramolecular chemistry.

As a result of our strategy 20 new complexes have been synthesized and characterized by X-ray diffraction measurements.

The interesting features of the synthesized complexes have been confirmed through the publications they have been the subject of:

-three families of $[M^{II}Ln^{III}]$ (M^{II} = Zn(II), Ni(II) and Cu(II)) binuclear complexes synthesized by using two non-compartmental Schiff-base ligands, Hvalampy and Hvalaepy, displaying interesting magnetic ($Ni^{II}Ln^{III}$, $Cu^{II}Ln^{III}$) and luminescence properties ($Zn^{II}Ln^{III}$);[108]

-Two mononuclear Fe(III) and a tetranuclear oxo-bridged $[Fe(III)Gd(III)]_2$ complex synthesized by using classical bicompartmental ligand, H_2valpn, displaying interesting magnetic and inclusion properties;[109]

-A dinuclear Fe(III) complex bridged by the dianion of trimesate linker, which has been synthesized from classical bicompartmental ligand, $H_2valdmpn$, shows interesting magnetic properties.[110]

The first part of the thesis deals with the relevant literature data: Chapter 1 gives a brief introduction about Schiff-base ligands and their classification. The compartmental Schiff-base ligands synthesized from *o*-vanillin and various diamines and their use as ligands to generate homo- and heterometallic 3d–3d' complexes, 3d–4f complexes and the generation of supramolecular assemblies through second coordination sphere interactions have been discussed in detail through relevant examples, with the emphasis placed on the structural, magnetic and luminescence properties of such systems.

The second part of the thesis deals with the original contributions. The experimental part begins with the description of two families of [Zn^{II}Ln^{III}] binuclear complexes, [Zn(valampy)$_2$Ln] and [Zn(valaepy)$_2$Ln] and the discussion of the luminescence properties of 3d–4f binuclear complexes belonging to [Zn(valampy)$_2$Ln] family of complexes has been presented (Chapter 2). The Chapter 3 describes two families of [Ni^{II}Ln^{III}] binuclear complexes, [Ni(valampy)$_2$Ln] and [Ni(valaepy)$_2$Ln] and their magnetic properties, in which the most interesting case is that of [Ni(valaepy)$_2$Gd] derivative which shows the occurrence of ferromagnetic interactions among the Ni^{II} and Gd^{III} ions. The Chapter 4 is concerned with [Cu^{II}Ln^{III}] binuclear complexes, [Cu(valaepy)$_2$Ln] and the magnetic properties of [Cu(valaepy)$_2$Gd] derivative, in which ferromagnetic interactions operate among the Cu^{II} and Gd^{III} ions. The Chapter 5 describes mononuclear Fe(III) and tetranuclear [Fe(III)Gd(III)]$_2$ complexes derived from classical bicompartmental Schiff-base ligand, H$_2$valpn and a dinuclear Fe(III) complex bridged by the dianion of trimesic acid, derived from the related classical bicomaprtmental ligand, H$_2$valdmpn. The magnetic properties of these complexes have been emphasized in accordance with their structures. The last chapter (6) of the original part describes a novel hexanuclear Cu(II) complex synthesized from a classical end-off compartmental ligand containing additional funtionalities.

The important conclusions drawn after taking into consideration theoretical and experimental data are presented in Chapter 7, which is followed by the annexes containing relevant experimental details and scientific results.

Objectives of the thesis

Several 3d−4f binuclear complexes have been described in the literature, which have been synthesized by using classical bicompartmental Schiff-base ligands derived from 2:1 condensation of *o*-vanillin and a diamine, exhibiting interesting magnetic and luminescence properties.[28]

In order to further enrich the library of Schiff-base ligands derived from *o*-vanillin which can be used to synthesize 3d−4f binuclear complexes, we have synthesized two new tetradentate non-compartmental Schiff-base ligands, Hvalampy (N-[(2-pyridyl)-methyl]-3-methoxy-

salicylimine) and Hvalaepy (N-[(2-pyridyl)-ethyl]-3-methoxy-salicylimine), which are obtained by 1+1 condensation of *o*-vanillin with 2-aminomethyl-pyridine and 2-(2-aminoethyl)-pyridine, respectively, as shown in Scheme 2.1.

HL^1 = Hvalampy
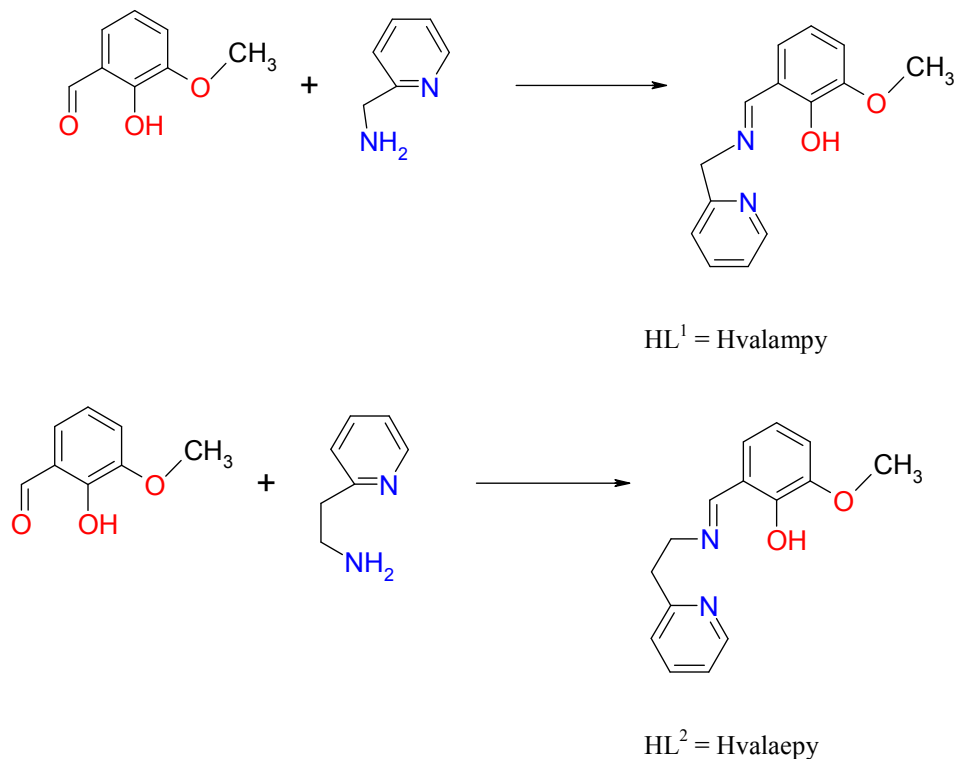
HL^2 = Hvalaepy

Scheme 2.1. Synthesis of tetradentate Schiff-base ligands HL^1 (Hvalampy) and HL^2 (Hvalaepy) used to synthesize [M^{II}Ln^{III}] heterodinuclear complexes.

By utilizing the two ligands, Hvalampy and Hvalaepy, we have synthesized five new series of heterodinuclear [Zn^{II}Ln^{III}], [Ni^{II}Ln^{III}] and [Cu^{II}Ln^{III}]complexes, which are discussed in Chapter 2, 3 and 4.

The structure of thesis

The thesis has been structured by an introductory part, which describes the relevant literature data (Chapter 1), a second part which presents the original contributions (Chapters 2 – 6), and the Conclusions (Chapter 7), and a final part which contains the supplementary data.

The theoretical part consists of two sections. In the first section a brief introduction of Schif-base ligands and their complexes is given and their relevant role is discussed which is followed by a brief classification of compartmental Schiff-base ligands. In the second section relevant examples of compartmental Schiff-base ligands derived from *o*-vanillin along with their use in the synthesis of homo- and heterometallic 3d–3d' complexes, 3d − 4f complexes and supramolecular assemblies designed by utilization of second coordination sphere interactions are discussed in detail.

The theoretical part of the thesis is followed by the original part, which contains five main chapters, numbered 2 − 6.

ORIGINAL CONTRIBUTIONS

2. Chapter 2. Heterodinuclear [Zn^{II}Ln^{III}] Complexes with Luminescent Properties

The chapter 2 describes two families of heterodinuclear [Zn^{II}Ln^{III}] complexes derived from two non-compartmental Schiff-base ligands, Hvalampy and Hvalaepy which are synthesized by 1:1 condensation of *o*-vanillin and 2-aminomethyl-pyridine and 2-(2-aminoethyl)-pyridine, respectively, and their spectroscopic and photoluminescent properties have been discussed.

2.1 Synthetic Strategy

The two series of [Zn^{II}Ln^{III}] heterodinuclear complexes have been synthesized *in-situ* in a step-wise manner without the isolation of mononuclear complex. The reaction of stoichiometric amounts of *o*-vanillin (2 mmol), 2-aminomethyl-pyridine or 2-(2-aminoethyl)-pyridine (2 mmol), in acetonitrile solvent, with Zn(NO$_3$)$_2$·6H$_2$O (1 mmol) and followed by Ln(NO$_3$)$_3$·nH$_2$O (1 mmol) in the presence of triethyl amine, (Et$_3$N) (4.8 mmol) resulted in the formation of desired products, as shown in Scheme 2.3.

2 [3-methoxy-2-hydroxybenzaldehyde] + 2 [2-(aminomethyl)pyridine] + Zn(NO$_3$)$_2$·6H$_2$O + Ln(NO$_3$)$_3$·nH$_2$O $\xrightarrow[\text{CH}_3\text{CN}]{\text{Et}_3\text{N}}$ [Zn(valampy)$_2$Ln(NO$_3$)$_3$]·CH$_3$CN

(a)

2 [3-methoxy-2-hydroxybenzaldehyde] + 2 [2-(2-aminoethyl)pyridine] + Zn(NO$_3$)$_2$·6H$_2$O + Ln(NO$_3$)$_3$·nH$_2$O $\xrightarrow[\text{CH}_3\text{CN}]{\text{Et}_3\text{N}}$ [Zn(valaepy)$_2$Ln(NO$_3$)$_3$]·CH$_3$CN
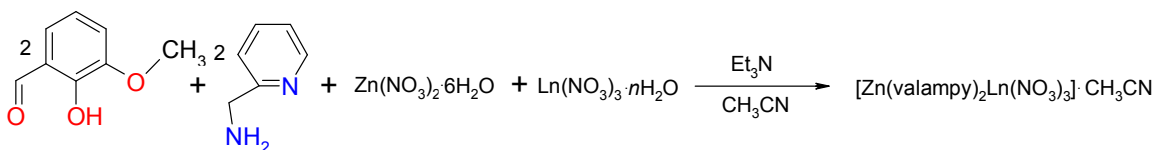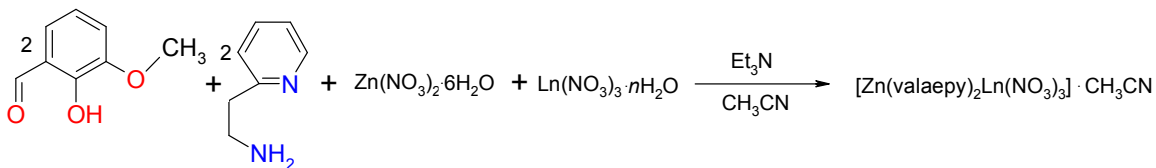
(b)

Scheme 2.3. (a) Synthesis of heterodinuclear [Zn^{II}(valampy)$_2$Ln^{III}] complexes (b) Synthesis of heterodinuclear [Zn^{II}(valaepy)$_2$Ln^{III}] complexes.

2.2 The [Zn^{II}(valampy)$_2$Ln^{III}] Family of Heterodinuclear Complexes

The complexes derived from Hvalampy ligand have the general formula, [Zn(valampy)$_2$Ln^{III}(O$_2$NO)$_3$]·CH$_3$CN (Ln^{III} = Sm **1**, Eu **2**, Gd **3**, Tb **4**, Dy **5**) and crystallize in the $C2/c$ monoclinic space group. All the synthesized complexes are isostructural and consist of a neutral dinuclear unit [Zn(valampy)$_2$Ln^{III}(O$_2$NO)$_3$] and an CH$_3$CN solvent molecule. Due to the isostructural nature of these heterodinuclear [Zn^{II}Ln^{III}] complexes, only the crystal structure of [Zn(valampy)$_2$Sm(O$_2$NO)$_3$]·CH$_3$CN, **1** (Figure 2.5) will be further illustrated.

2.2.1 Crystallographic Measurements and Structure Description

The X-ray crystal structure analysis shows that the [Zn^{II}Ln^{III}] heterodinuclear complex, [Zn(valampy)$_2$Sm(O$_2$NO)$_3$]·CH$_3$CN **1,** consists of a neutral dinuclear unit [Zn(valampy)$_2$Sm(O$_2$NO)$_3$] and an CH$_3$CN solvent molecule. Within the dinuclear unit, the zinc ion shows a strongly distorted geometry, with two long bonds (involving the pyridyl nitrogen atoms, Zn1 – N2 = 2.3956(16) Å), and four short bonds (involving the azomethenic nitrogen and the phenoxo oxygen atoms: Zn1 – N1 = 2.0603(14); Zn1 – O2 = 2.0504(10) Å). Since the coordination sphere for a d^{10} ion is more flexible than that of Ni(II) (see chapter 3), the two

methoxy groups from the two valampy ligands come closer to the lanthanide cations (for example, in **1**: Sm1 – O1 = 2.7024(13) Å), (Figure 2.5).
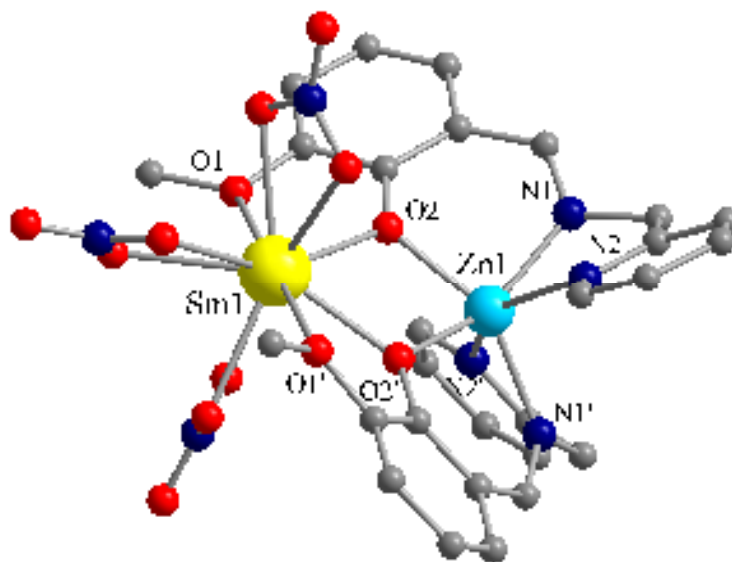
Figure 2.5. Molecular structure of [Zn(valampy)$_2$Sm(O$_2$NO)$_3$] in crystal **1** (' = -*x*, *y*, 1.5-*z*).

The samarium ion which is located in the open O$_2$O'$_2$ compartment, exhibits a coordination number of eight: two phenoxo bridging oxygen atoms arise from two Schiff-base ligand moieties [Sm1 – O2 = 2.3551(10) Å] and two oxygen atoms originate from each of the three chelating nitrato ions [Sm1 – O5 = 2.5395(13); Sm1 – O7 = 2.5189(15); Sm1 – O9 = 2.5022(14) Å]. The two methoxy groups can be considered as being semi-coordinated [Sm1 – O1 = 2.7024(13)]. The intermetallic Zn⋯Sm separation is equal to 3.594 Å.

2.2.2. Spectral characterization of [Zn^{II}(valampy)$_2$Ln^{III}] Complexes

These complexes have been spectroscopically characterized. The IR data of the heterodinuclear [Zn^{II}(valampy)$_2$Ln^{III}] complexes show the presence of the characteristic bands of the organic ligand, solvent molecules and nitrato groups attached to the lanthanide ion. For example, in the IR spectrum (Figure 2.8) of [Zn(valampy)$_2$Sm(O$_2$NO)$_3$]·CH$_3$CN, **1**, the occurrence of a strong band at 1384 cm^{-1} shows the presence of chelating nitrato ligands in the

coordination sphere of lanthanide ion. The sharp, medium intensity band at 1644 cm^{-1} in the spectrum of **1** arises from C=N stretching vibrations, ν(C=N) of the imine group of the organic ligand. The presence of a medium intensity band at 1311 cm^{-1} is attributed to the stretching vibrations of the phenoxo group, ν(C–O) of the organic ligand. A medium intensity peak at 1473 cm^{-1} represents the superposition of the corresponding vibrational frequencies of the aromatic ring of the organic ligand, ν(C=C), and the coordinated nitrato ligands, ν_{asim}(NO$_2$).
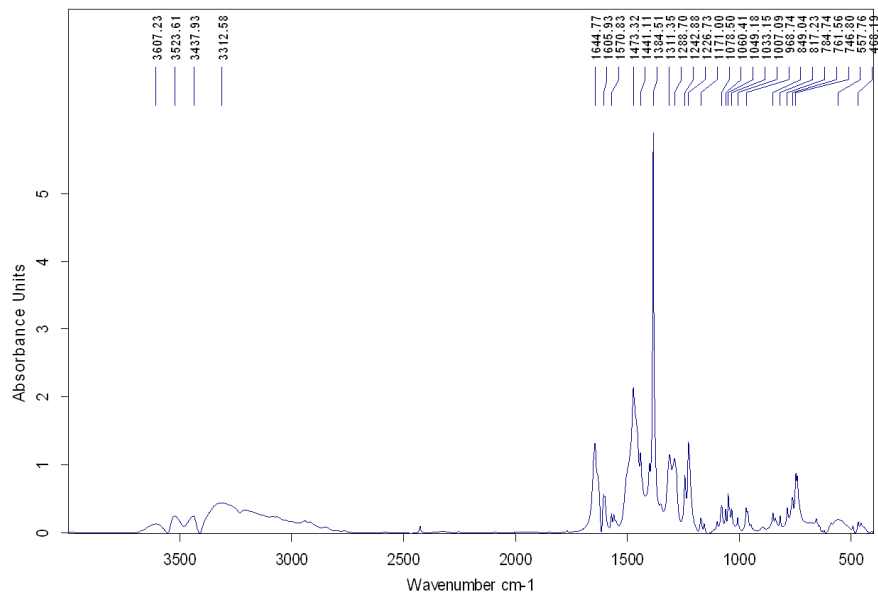
Figure 2.8. The IR spectrum of [Zn(valampy)$_2$Sm(O$_2$NO)$_3$]·CH$_3$CN, **1**

The analysis of the UV-Vis-NIR spectra of [Zn^{II}(valampy)$_2$Ln^{III}] complexes, showed, in all cases, the presence of a structured absorption band in the UV range which corresponds to the π–π* transitions of the Schiff-base ligand. The large structured absorption band is composed of two peaks of increasing intensity following the order: 275 nm < 350 nm, and a shoulder at 450 nm. The 3d metal ion, Zn^{2+} has complete 3d^{10} configuration and therefore it does not exhibit d–d transitions.

The characteristic f–f transitions for the Ln^{3+} ions have been observed for the lanthanide ions (Sm^{3+}, Dy^{3+}). In the case of Tb^{3+}, the characteristic f–f transitions appear below 390 nm, a region which is masked by the strong absorption bands of the organic ligand. Similarly in the

case of Eu^{3+}, the characteristic f–f transitions lie in the 360–400 nm range, a region of spectrum which is masked by the strong absorption bands arising from the organic ligands, whereas the Gd^{3+}, having half-filled 4f shell of electrons $(4f^7)$ cannot exhibit these transitions.
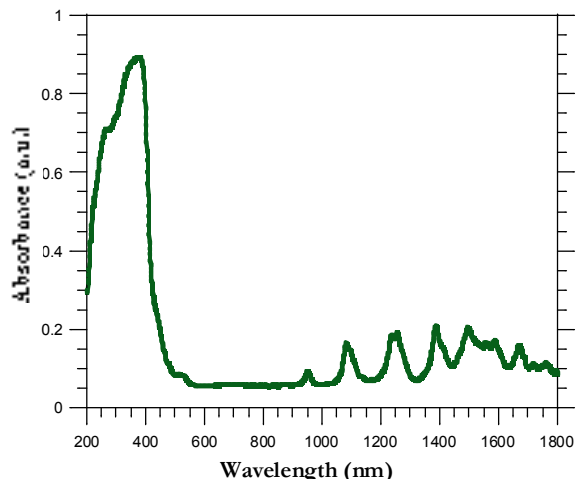
Figure 2.9. The electronic spectrum of $[Zn(valampy)_2Sm(O_2NO)_3]\cdot CH_3CN$, **1**.

2.2.3. Photophysical Properties of $[Zn^{II}(valampy)_2Ln^{III}]$ Complexes

The most important features of the $[Zn(valampy)_2Ln]$ complexes are their photoluminescent properties. Some of the lanthanide ions display strong luminescent emissions in the visible (Sm^{III}, Tb^{III}, Eu^{III}, Dy^{III}) or NIR (Nd^{III}, Er^{III}, Yb^{III}) range. As the f–f transitions are parity forbidden, the molar absorption coefficients are normally very low, and the emissive rates are slow. However, this disadvantage can be overcome by the use of suitably designed organic ligands (chromophores) which can act as sensitizers to excite lanthanide ions (*antenna effect*). The Schiff-base ligand, valampy⁻, which we have used has been shown to behave like an *antenna*.

17

2.2.3.1. Luminescence of Sm^{III} Complex

In the case of [Zn(valampy)$_2$Sm^{III}(O$_2$NO)$_3$]·CH$_3$CN **1**, and [Zn(valampy)$_2$Tb^{III}(O$_2$NO)$_3$]·CH$_3$CN **4** complexes, the excitation spectra showed the presence of ligand-centered bands thus confirming an *antenna effect*. Both the Sm^{III} and Tb^{III} derivatives gave a strong orange-red and green luminescent emission, respectively, which are observable with the naked eye, following excitation with a standard UV lamp (λ_{ex} = 365 nm). In the excitation spectrum of the samarium complex **1**, the most intense band corresponds to the ligand-centered electronic transition, indicating for an efficient ligand to metal energy transfer. The ligand-to-metal energy transfer occurs via the triplet states $^3\pi\pi^*$ of the ligand directly to the $^4G_{5/2}$ level of Sm^{III}. The intensity ratio of 2.1 between the predominantly electric dipole transition, $^4G_{5/2}$-$^6H_{9/2}$ and $^4G_{5/2}$-$^6H_{5/2}$ transition, having predominant magnetic dipole character is indicative of the departure from centrosymmetry, which is in line with the distorted polyhedron around Sm(III) as determined with the X-ray data.
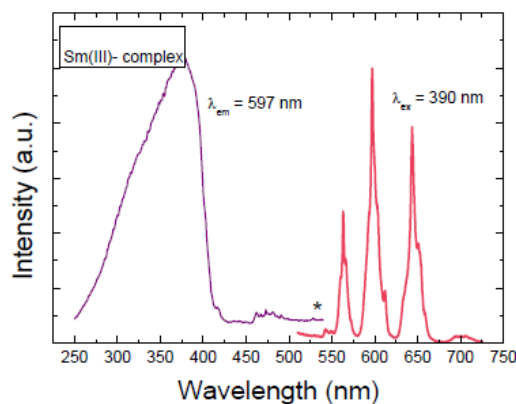
Figure 2.14. Excitation (λ_{em} = 597 nm) and emission spectra of Sm complex (λ_{ex} = 390 nm).

2.2.3.2. Luminescence of Eu^{III} Complex

The europium complex **2**, exhibits the weak emission bands indicating an inefficient energy transfer from the triplet state of the ligand to europium(III) emissive level, $^5D_0$. This is confirmed by the presence of weak ligand-centered absorption in the excitation spectrum indicating weak sensitization of europium emission by the ligands. This weak sensitization of europium emission is due to the non-radiative relaxation of Eu(III) emission by the ligand-to-

metal charge transfer (LMCT) state due to the strong electron donating ability of the Schiff-base ligand and the strong reduction tendency of Eu(III) to Eu(II).
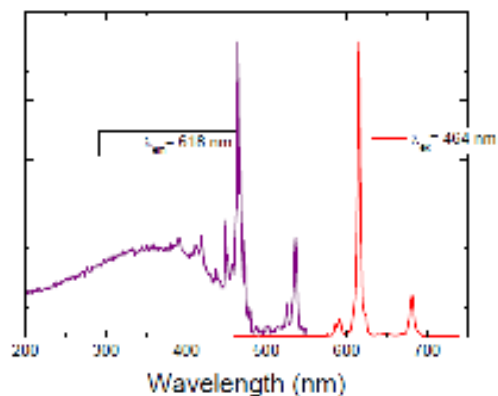
Figure 2.15. Excitation (λ_{em} = 618 nm) and emission spectra of Eu(III) complex.

2.2.3.3. Luminescence of Gd[III] Complex

In case of the Gd[III] derivative **3**, only the band due to ligand $\pi^*-\pi$ fluorescence is observable, due to the reason that the emissive level of Gd[III] lies at higher energy than the ligand triplet state and therefore energy can not be transferred from ligand triplet state to the emissive level of the Gd[III] ion.
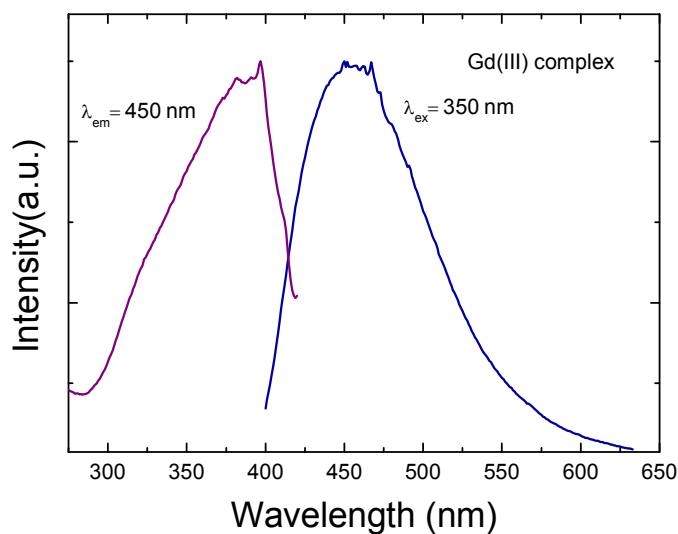
Figure 2.16. Excitation and emission spectra of Gd(III) complex **3**.

2.2.3.4. Luminescence of Tb[III] Complex

In case of terbium(III) complex, [Zn(valampy)$_2$Tb(O$_2$NO)$_3$]·CH$_3$CN, **4**, relatively strong green emission was observed and no broad, ligand related emission was observed. The excitation spectrum showed strong ligand-centered bands with a pronounced "valley" spectral feature, indicating an efficient ligand to metal energy transfer process. The rather short lifetime, τ, of 500 μs indicates for strong non-radiative quenching of the metastable $^5D_4$ state emission as generally the terbium lifetimes with no bound water molecules in the first coordination sphere lie in the ms range. The increase of the lifetime from 500 μs at room-temperature to 1.3 ms at liquid nitrogen temperature confirmed the dominant contribution of a temperature-*dependent* vibrational quenching.
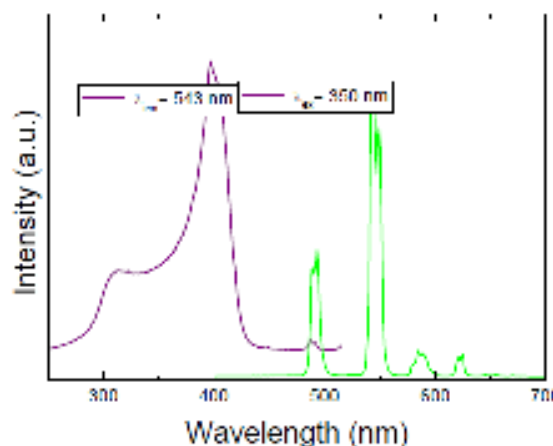
Figure 2.17. (a) Excitation (λ_{em} = 544 nm) and emission spectra of Tb(III) complex (λ_{ex} = 390 nm).

2.2.3.5. Luminescence of Dy[III] Complex

In the case of dysprosium derivative, [Zn(valampy)$_2$Dy(O$_2$NO)$_3$]·CH$_3$CN, **5**, the emission and excitation spectra point to an inefficient ligand to metal energy transfer process. The intensity ratio of 9.05 between the $^4F_{9/2}$-$^6H_{13/2}$ transition, with the predominant electric dipole character and $^4F_{9/2}$-$^6H_{11/2}$, with predominant magnetic dipole character is in line with the distorted symmetry at Dy(III) sites found by X-ray analysis. The emission/excitation spectra together with the relative short, lifetime of roughly 1μs suggest that the energy gap is not large enough to

prevent the back-transfer of excitation from the excited level of Dy(III) to the triplet state of the ligand at room-temperature.
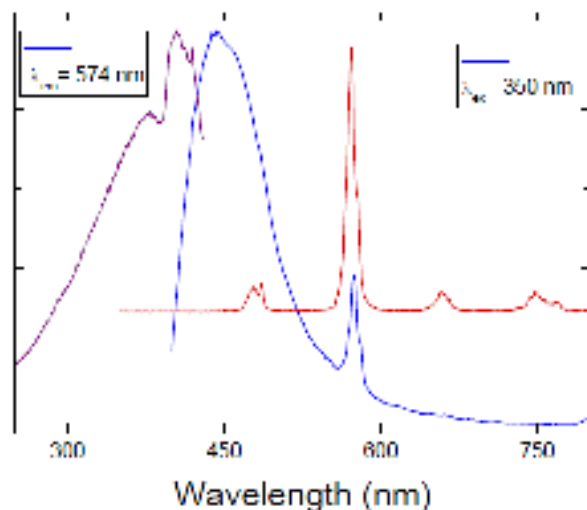
Figure 2.18. Excitation (λ_{em} = 574 nm) and emission spectra of Dy complex. Spectrum 1 is measured under steady-state excitation at λ_{ex}= 350 nm; spectrum 2 is measured under pulsed laser excitation at λ_{ex}= 390 nm, initial delay δt = 1 μs.

2.3. The [Zn^{II}(valaepy)$_2$Ln^{III}] Heterodinuclear Complex

The second family of [Zn^{II}Ln^{III}] complexes has been synthesized by utilizing the other Schiff-base ligand, Hvalaepy (obtained by 1:1 condensation of o-vanillin and 2-(2-aminoethyl)-pyridine), having the general formula [Zn(valaepy)$_2$Ln^{III}(O$_2$NO)$_3$]·CH$_3$CN (Ln^{III} = Sm **6**) and crystallizes in the $P2_1/c$ monoclinic space group. The X-ray crystal structure was solved for Sm derivative, **6**.

2.3.1. Crystallographic Measurements and Structure Description

The X-ray crystal structure analysis shows that the [Zn^{II}Ln^{III}] heterodinuclear complex, [Zn(valaepy)$_2$Sm(O$_2$NO)$_3$]·CH$_3$CN **6,** consists of a neutral dinuclear [Zn(valaepy)$_2$Sm(O$_2$NO)$_3$] unit and an CH$_3$CN solvent molecule. The crystal structure is constructed from Zn(II) and Sm(III) ions which are connected through a double bridge formed by the two phenoxo oxygen atoms [O(2), O(4)] arising from two Schiff-base ligand moieties, [L^2]$^-$ (valaepy). The four

atoms, Sm1-O2-Zn1-O4, can be considered as approximately coplanar, the dihedral angle between the planes Sm1-O2-Zn1 and Sm1-O4-Zn1 being equal to 1.34°. The Zn···Sm distance is equal to 3.5871(6) Å. The bond angles Zn1-O2-Sm1 and Zn1-O4-Sm1 slightly differ from each other, having the values of 107.40(12)° and 110.61(13)°, respectively. The bond lengths Zn-O(phenoxo) differ by a value of 0.014 Å, whereas the difference in the bond lengths of Sm-O(phenoxo) is equal to 0.097 Å.
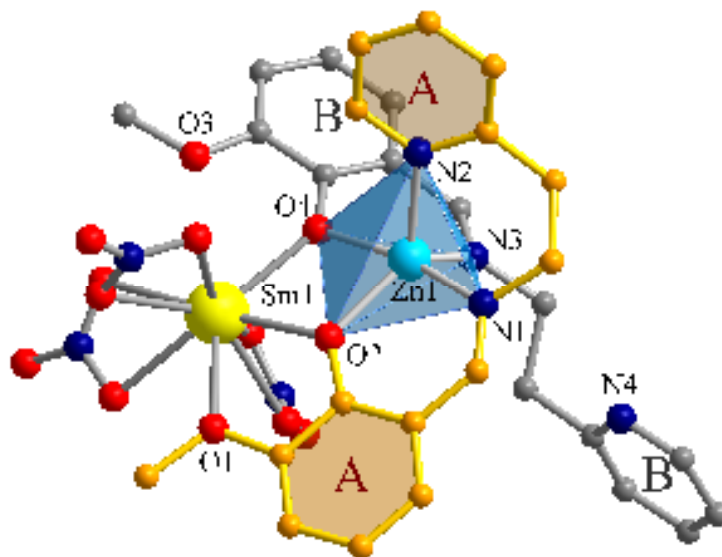
Figure 2.19. View of the molecular structure of [Zn(valaepy)$_2$Sm(O$_2$NO)$_3$] in **6**.

The crystallographic investigation of **6** (Figure 2.19) reveals that the coordination modes of the two ligand molecules towards zinc are different: one of them (valaepy-**A**) is coordinated to the zinc ion through the phenoxo oxygen atom and the two nitrogen atoms, while the second one (valaepy-**B**) is coordinated through the phenoxo oxygen and the azomethenic nitrogen, the pyridyl arm being uncoordinated. Consequently, the zinc ion is pentacoordinated, with trigonal bipyramidal geometry. The trigonal plane is made by one oxygen (Zn1 – O2 = 2.033(3) Å) and by two nitrogen atoms arising from the pyridyl group of the valaepy-**A** ligand (Zn1 – N2 = 2.102(4) Å) and by the azomethenic nitrogen arising from the valaepy-**B** ligand (Zn1 – N3 = 2.071(4) Å). The apical positions are occupied by a phenoxo oxygen (Zn1 – O4 = 2.047(3) Å), and by a nitrogen atom from the tridentate valaepy ligand Zn1 – N1 = 2.037(4) Å). The samarium ion is located into the open cavity described by the four oxygen atoms arising from the

two ligand molecules. The methoxy group from valaepy-**A** is coordinated to the samarium ion (Sm1 – O1 = 2.544(3) Å), while the other one, arising from the valaepy-**B** molecule, can be considered as semicoordinated (Sm1 – O3 = 2.900(4) Å). Taking into account only the samarium – oxygen distances in the range 2.4 – 2.6 Å, the samarium ion is nine-coordinated: two bridging phenoxo oxygens, six oxygen atoms from the bidentate nitrato ligands, and one oxygen from the methoxy group. The intramolecular distance between the metal centers is: Zn···Sm = 3.5871(6) Å.

The crystal structure analysis of $[Zn(valaepy)_2Sm(O_2NO)_3]\cdot CH_3CN$ **6**, reveals significant differences in the structure of complexes belonging to the two families of heterodinuclear complexes, $[Zn^{II}(valampy)_2Ln^{III}]$ and $[Zn^{II}(valaepy)_2Ln^{III}]$, respectively. In case of heterodinuclear $[Zn^{II}(valampy)_2Ln^{III}]$ family of complexes, the Zn^{II} ion is hexacoordinated and adopts a distorted octahedral coordination geometry and the lanthanide ion is eight coordinated, whereas in the case of $[Zn^{II}(valaepy)_2Ln^{III}]$ complex, the Zn^{II} ion is penta-coordinated and is situated in the distorted trigonal bipyramidal coordination geometry and the lanthanide ion is nine coordinated with one methoxy oxygen atom (O3) being semicoordinated.

2.3.2. Spectral characterization of $[Zn^{II}(valaepy)_2Ln^{III}]$ Complex

The heterodinuclear $[Zn(valaepy)_2Sm^{III}(O_2NO)_3]\cdot CH_3CN$ **6** complex has been spectroscopically characterized. In the IR spectrum of $[Zn(valaepy)_2Sm(O_2NO)_3]\cdot CH_3CN$, **6**, the occurrence of a strong band at 1384 cm^{-1} indicates the presence of chelating nitrato ligands in the coordination sphere of lanthanide ion. The sharp, medium intensity band at 1626 cm^{-1} in the spectrum of **6** arises from C=N stretching vibrations, ν(C=N) of the imine group of the organic ligand. The presence of a medium intensity band at 1302 cm^{-1} is attributed to the stretching vibrations of the phenoxo group, ν(C–O) of the organic ligand. A strong peak at 1470 cm^{-1} is indicative of the overlapping of the corresponding vibrational frequencies of the aromatic ring of the organic ligand, ν(C=C), and the coordinated nitrato ligands, $\nu_{asim}(NO_2)$.

The UV-Vis-NIR spectrum of $[Zn^{II}(valaepy)_2Ln^{III}]$ complex has been recorded. In the electronic spectrum of $[Zn(valaepy)_2Sm(O_2NO)_3]\cdot CH_3CN$, **6**, the broad absorption band (200–

430 nm) consists of two overlapping peaks with increasing intensities of 275 nm < 360 nm, and is extended into the visible region by a shoulder at 450 nm. The broad absorption band arises due to the π–π* transitions of the Schiff-base ligand moieties. The sharp absorption peaks occurring at 950 nm, 1090 nm, 1230 nm, 1250 nm, 1400 nm and 1665 nm, respectively, arise from the electronic transitions of the Sm^{III} ion. The strong NIR bands at 1090 nm and 1250 nm can be attributed to the spin-allowed ($\Delta S = 0$) $^6H_{5/2} - {}^6F_{9/2}$ and $^6H_{5/2} - {}^6F_{7/2}$ transitions, respectively.

3.   Chapter 3. Heterodinuclear [$Ni^{II}Ln^{III}$] Complexes with Magnetic Properties

Chapter 3 describes two families of heterodinuclear [$Ni^{II}Ln^{III}$] complexes, which have been synthesized by using Schiff-base ligands, Hvalampy and Hvalaepy, which are obtained from 1:1 condensation of o-vanillin and 2-aminomethyl-pyridine or 2-(2-aminoethyl)-pyridine, respectively.

3.1.   Synthetic Strategy

The reaction of stoichiometric amounts of o-vanillin (2 mmol), 2-aminomethyl-pyridine or 2-(2-aminoethyl)-pyridine (2 mmol), in acetonitrile solvent, with $Ni(NO_3)_2 \cdot 6H_2O$ (1 mmol) and $Ln(NO_3)_3 \cdot nH_2O$ (1 mmol) in the presence of triethyl amine, (Et_3N) (4.8 mmol) resulted in the formation of desired products.

3.2. The [$Ni^{II}(valampy)_2Ln^{III}$] Family of Heterodinuclear Complexes

In the [$Ni^{II}(valampy)_2Ln^{III}$] complexes, two structural types based on X-ray crystallographic data of the dinuclear complexes are observed, which differ on the basis of the coordination number and environment of the lanthanide ion and the type of solvent molecules. The type I has the general formula [$Ni(valampy)_2Ln(O_2NO)_3(H_2O)_2$]·$2H_2O$ (Ln^{III} = La (**7**), Sm (**8**)), in which the lanthanide ion is ten coordinated and two water molecules act as solvent

molecules of crystallization. The type I structure is represented by **8**, which will be further illustrated as a representative example.

3.2.1. Crystallographic Measurements and Structure Description

The samarium derivative **8**, crystallizes in the *C2/n* monoclinic space group and is consisted of neutral dinuclear [Ni(valampy)$_2$Sm(O$_2$NO)$_3$(H$_2$O)$_2$]·2H$_2$O entities as shown in Figure 3.2).
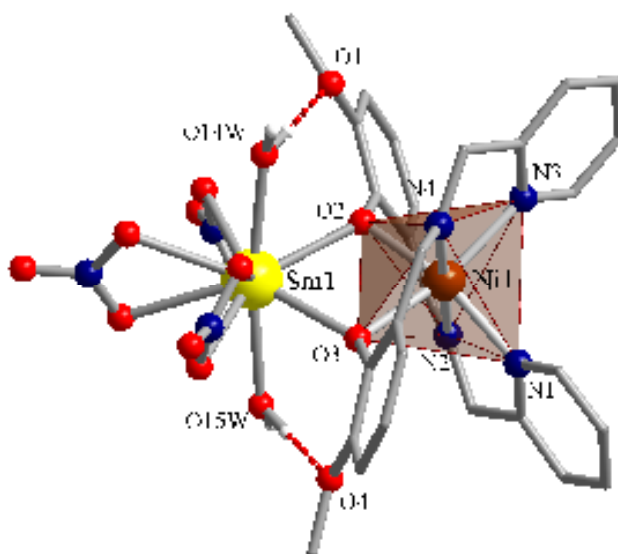
Figure 3.2. Perspective view of [Ni(valampy)$_2$Sm(O$_2$NO)$_3$(H$_2$O)$_2$] in **8**.

The nickel ion is located in an octahedral coordination environment, with the N$_2$O$_2$ tetragonal base constructed from two nitrogen atoms arising from pyridyl groups of the two Schiff-base ligand moieties [Ni1 – N1 = 2.112(3); Ni1 – N3 = 2.120(3) Å] and two phenoxo oxygen atoms [Ni1 – O2 = 2.063(2); Ni1 – O3 = 2.081(2) Å], whereas, the two nitrogen atoms arising from azomethenic groups of the two Schiff-base ligand moieties [Ni1 – N2 = 2.032(2); Ni1 – N4 = 2.026(3) Å] occupy the axial positions.

The samarium ion is located in the large, open compartment, which is formed by the coordination of two Schiff-base ligand moieties with the 3d metal ion. The samarium ion is surrounded by ten oxygen atoms: the two bridging phenoxo oxygen atoms arise from two Schiff-base ligand moieties [Sm1 – O2 = 2.434(2); Sm1 – O3 = 2.401(2) Å], the two oxygen atoms arise from two coordinated water molecules [Sm1 – O14w = 2.460(2); Sm1 – O15w = 2.476(2) Å] and two oxygen atoms arise from each of the three chelating nitrato ions [Sm1 – O5 = 2.564(3); Sm1 – O6 = 2.567(2); Sm1 – O8 = 2.566(2); Sm1 – O9 = 2.582(3); Sm1 – O11 = 2.551(3); Sm1 – O12 = 2.627(3) Å]. The aqua ligands are involved in intramolecular hydrogen bond interactions with the methoxy oxygen atoms, O14w⋯O1 = 2.780(4) Å and O15w⋯O4 = 2.793(4) Å.

At the supramolecular level, the dinuclear units are arranged to form a 1 D chain, through the establishment of hydrogen bonding interactions between the oxygen atom of water molecule (O14w) of one dinuclear unit and the oxygen atom (O6) of one of the nitrato ions belonging to the adjacent dinuclear unit, resulting in the formation of double bridge between the two dinuclear units [O14w'⋯O6 = 2.83 Å; ' = 1-x, -y, 1-z]. Similarly, the oxygen atom of other water molecule (O15w) coordinated to the lanthanide ion of one dinuclear unit forms hydrogen bonding interactions with the oxygen atom (O8) of one of the nitrato ions belonging to the adjacent dinuclear unit [O15w'⋯O8 = 2.88 Å; ' = 1.5-x, 0.5-y, 1-z], and a double hydrogen bonding bridge is formed between the adjacent dinuclear units, thereby resulting in the formation of a 1 D chain as shown in Figure 3.4.
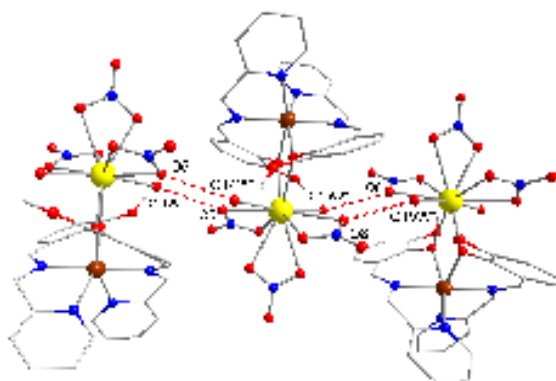
Figure 3.4. Packing diagram of **8** showing the formation of 1D supramolecular chains (' = 1-x, -y, 1-z; " = 1.5-x, 0.5-y, 1-z).

The type II structure has the general formula $[Ni(valampy)_2Ln(O_2NO)_3(H_2O)]\cdot2CH_3CN$ (Ln^{III} = Eu (**9**)), and in this structural type the lanthanide ion exhibits a coordination number of nine, and two acetonitrile molecules act as solvent molecules of crystallization. Compound **9** has a type II structure and crystallizes in the triclinic *P-1* space group. The crystal structure analysis shows that the complex $[Ni(valampy)_2Eu(O_2NO)_3(H_2O)]\cdot2CH_3CN$ **9**, consists of a neutral heterodinuclear $[Ni(valampy)_2Eu(O_2NO)_3(H_2O)]$ unit and two CH_3CN molecules as solvent molecules of crystallization (Figure 3.5).

The Ni^{II} ion is situated in the octahedral coordination environment, with the N_2O_2 tetragonal base formed by the two nitrogen atoms arising from pyridyl groups of the two Schiff-base ligand moieties [Ni1 – N2 = 2.099(8); Ni1 – N4 = 2.114(10) Å] and two oxygen atoms [Ni1 – O2 = 2.076(7); Ni1 – O4 = 2.119(8) Å], whereas the two nitrogen atoms arising from azomethenic groups of the two Schiff-base ligand moieties [Ni1 – N1 = 2.029(8); Ni1 – N3 = 2.019(8) Å] are located in the axial positions.
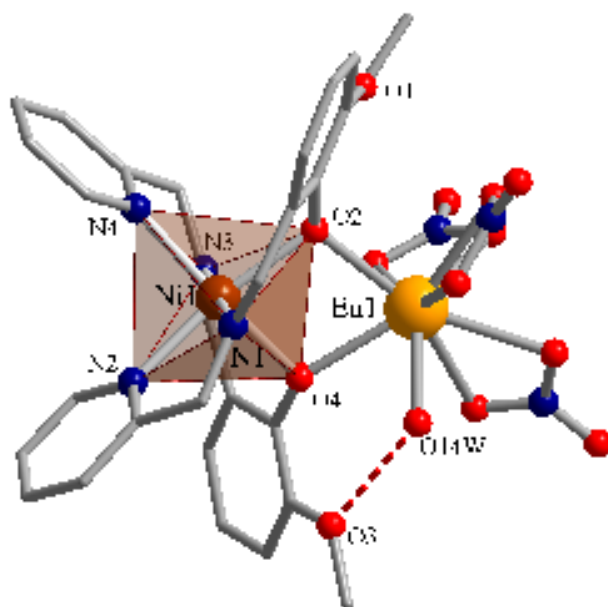
Figure 3.5. Perspective view of $[Ni(valampy)_2Eu(O_2NO)_3(H_2O)]$ in **9**.

The europium ion is located in the large, open compartment, which is formed by the coordination of two Schiff-base ligand moieties with the 3d metal ion. The europium ion is

surrounded by nine oxygen atoms, the two bridging phenoxo oxygen atoms [Eu1 – O2 = 2.335(8); Eu1 – O4 = 2.381(7) Å] originate from the two Schiff-base ligand moieties, one oxygen atom [Eu1 – O14w = 2.418(7) Å] from the coordinated water molecule, and two oxygen atoms [Eu1 – O5 = 2.502(8); Eu1 – O6 = 2.508(8); Eu1 – O8 = 2.564(7); Eu1 – O9 = 2.559(7); Eu1 – O11 = 2.520(10); Eu1 – O12 = 2.521(9) Å] arise from each of the three chelating nitrato ions. The aqua ligand is involved in intramolecular hydrogen bond interactions with one of the uncoordinated methoxy groups, O14w⋯O3 = 2.778(14) Å.

Interestingly, as in the case of samarium derivative **8**, the two methoxy groups are too far to be coordinated to the europium ion [Eu1⋯O1 = 3.98; Eu1⋯O3 = 4.07 Å]. In contrast to the samarium derivative, the europium ion exhibits a coordination number of nine in [Ni(valampy)$_2$Eu(O$_2$NO)$_3$(H$_2$O)]·2CH$_3$CN **9**. The intermetallic Ni⋯Eu separation is 3.4719(18) Å.

At the supramolecular level, the dinuclear units interact through hydrogen bonding interactions resulting in the formation of a supramolecular dimer of dinuclear units. The hydrogen bonds are established between the oxygen atom (O14w) of coordinated water molecule of one dinuclear unit and the oxygen atom (O5) of one of the nitrato ligands attached to the europium ion of the adjacent dinuclear unit, thereby resulting in the formation of double H-bonding bridge [O14w'⋯O5 = 2.82 Å; ' = 1-x, -y, -z] between the two dinuclear units and thus giving rise to a supramolecular dimer of dinuclear units (Figure 3.7).
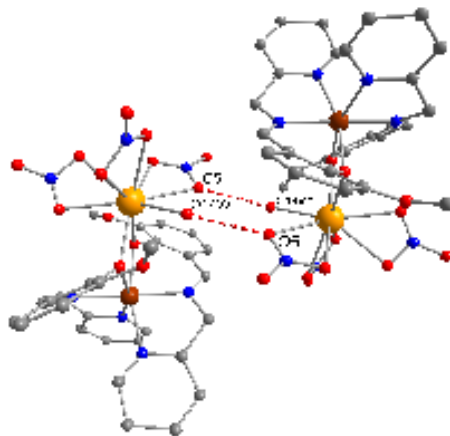

Figure 3.7. Packing diagram of **9** showing the formation of a supramolecular dimer of dinuclear units through the establishment of hydrogen bonding interactions (' = 1-x, -y, -z).

3.2.2. Spectral characterization of heterodinuclear [Ni^{II}(valampy)$_2$Ln^{III}] Complexes

The [Ni^{II}(valampy)$_2$Ln^{III}] complexes have been spectroscopically characterized. The IR data of the heterodinuclear [Ni^{II}(valampy)$_2$Ln^{III}] complexes show the presence of the characteristic bands of the organic ligand, nitrato groups attached to the lanthanide ion, and the solvent molecules. For example, in the IR spectrum of [Ni(valampy)$_2$La(O$_2$NO)$_3$(H$_2$O)$_2$]·2H$_2$O **7**, the occurrence of a strong band at 1384 cm^{-1} indicates the presence of chelating nitrato ligands attached to the lanthanide ion. A broad and medium intensity band at 3400 cm^{-1} indicates the presence of coordinated and crystallization water molecules. The sharp, medium intensity band at 1644 cm^{-1} in the spectrum arises from C=N stretching vibrations, ν(C=N) of the imine group of the organic ligand. A medium intensity peak at 1449 cm^{-1} (with a shoulder at 1471 cm^{-1}) represents the superposition of the corresponding vibrational frequencies of the aromatic ring of the organic ligand, ν(C=C), and the coordinated nitrato ligands, ν_{asim}(NO$_2$).

The UV-Vis-NIR spectra of [Ni^{II}(valampy)$_2$Ln^{III}] complexes have been recorded in the 200 – 1300 nm range. The electronic spectra of the complexes should exhibit the presence of three different chromophores: (i) the organic ligand moieties, valampy$^-$; (ii) the octahedrally coordinated Ni^{II} ion; (iii) the Ln^{III} ion. For example, the electronic spectrum of [Ni(valampy)$_2$La(NO$_3$)$_3$(H$_2$O)$_2$]·2H$_2$O **7**, exhibits a broad structured absorption band corresponding to the π–π* transitions of the Schiff-base ligand moieties. The broad, structured absorption band is made up of three overlapping peaks of increasing intensity as follows: 250 nm < 275 nm < 350 nm (Figure 3.9). This behaviour is similar to the one encountered in the case of [Zn^{II}(valampy)$_2$Ln^{III}] binuclear complexes discussed in the chapter 2.
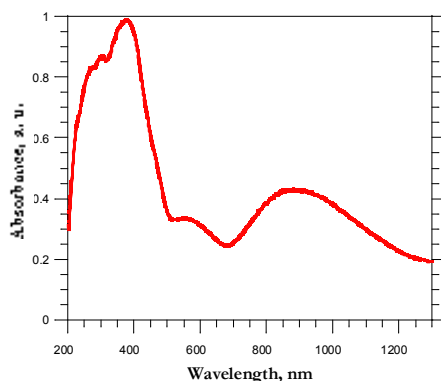
Figure 3.9. The electronic spectrum of [Ni(valampy)$_2$La(O$_2$NO)$_3$(H$_2$O)$_2$]·2H$_2$O, **7**.

The shoulder of absorption band in the region of 400 – 450 nm, indicates the presence of the band corresponding to the $^3A_{2g} \rightarrow {}^3T_{1g}(P)$ transition of Ni^{II} ion which corresponds to the highest energy (this band is most probably obscured by the π–π* bands). The d-d spin-allowed transitions of the Ni^{II} ion from the [NiN$_4$O$_2$] chromophore of complex **7** occur at 550 nm [$^3A_{2g} \rightarrow {}^3T_{1g}(F)$] and 850 nm [$^3A_{2g} \rightarrow {}^3T_{2g}$]. The weak absorption band corresponding to the spin-forbidden $^3A_{2g} \rightarrow {}^1E_g$ transition is not visible in the spectrum of [Ni(valampy)$_2$La(O$_2$NO)$_3$(H$_2$O)$_2$]·2H$_2$O **7**. No f–f absorption transitions are observed in the spectrum due to the reason that La^{III} has 4f^0 electron configuration.

3.2.3. Magnetic Properties of [Ni^{II}(valampy)$_2$Ln^{III}] Complexes

The molar magnetic susceptibility χ_M, for compounds **7–9** have been recorded in the temperature range of 2–300 K. The simplest case among the [Ni^{II}(valampy)$_2$Ln^{III}] complexes is that of the lanthanum derivative, **7**, in which the deviation from the Curie behaviour is explained on the basis of zero field splitting (ZFS) associated to the Ni^{II} ion.
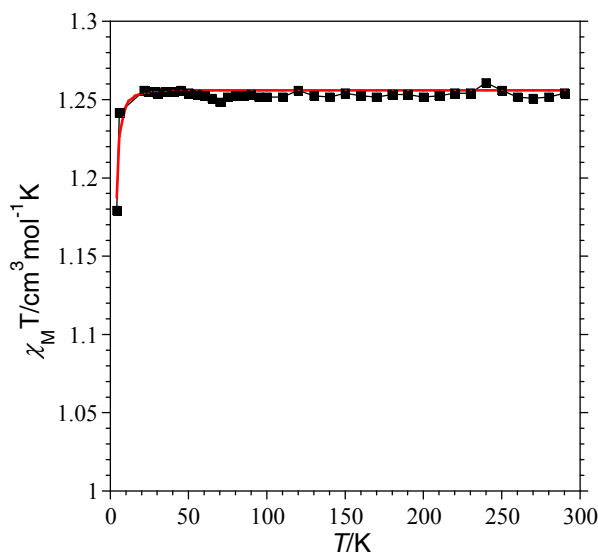

Figure 3.12. $\chi_M T$ curve for [Ni(valampy)$_2$La(O$_2$NO)$_3$(H$_2$O)$_2$]·2H$_2$O **7**. The red solid line represents the best fit to the data.

The magnetic properties of complexes containing lanthanide ions other than the La^{III} and Gd^{III} are more complicated due to the presence of the intervening first order angular momentum and crystal field effect of the Ln^{III} ions. For these compounds the variation of the magnetic behaviour results from the overlap of two phenomena. One results from the exchange interaction operating between Ni^{II} and Ln^{III} ions. The second is the intrinsic property of the Ln^{III} ion and originates from the thermal population of the Stark levels.[25]

3.3. The [Ni^{II}(valaepy)$_2$Ln^{III}] Family of Heterodinuclear Complexes

In the second family of heterodinuclear [Ni^{II}(valaepy)$_2$Ln^{III}] complexes, only one structural type is observed, which has the general formula [Ni(valaepy)$_2$Ln(O$_2$NO)$_3$(H$_2$O)]·CH$_3$CN (Ln^{III} = Eu **10**, Gd **11**, Dy **12**, Ho **13**). All the heterodinuclear complexes are isostructural, hence only the crystallographic structure of Eu^{III} derivative, **10** will be discussed further as a representative example.

3.3.1. Crystallographic Measurements and Structure Description

The europium derivative **10**, crystallizes in the monoclinic *P21/n* space group and is consisted of neutral dinuclear [Ni(valaepy)$_2$Eu(O$_2$NO)$_3$(H$_2$O)]·CH$_3$CN entities as shown in Figure 3.15. First of all, we notice that the nickel(II) ion is hexacoordinated, with an octahedral geometry. This stereochemistry is very characteristic for the hexacoordinated nickel ions. The coordination sphere is formed by two azomethenic and two pyridyl nitrogen atoms, and by two phenoxo oxygens, with bond distances varying between 2.080(2) and 2.1142(16) Å. The europium and nickel ions are bridged by two phenoxo oxygens. The coordination number of europium is 9 (two phenoxo oxygen atoms, six oxygens from three chelating nitrato ligands, and one aqua ligand). The bond distances vary between 2.3082(16) and 2.562(2) Å, the shortest bonds involving the phenoxo oxygen atoms (Eu1 – O2 = 2.3082(16); Eu1 – O4 = 2.3679(16) Å).

31
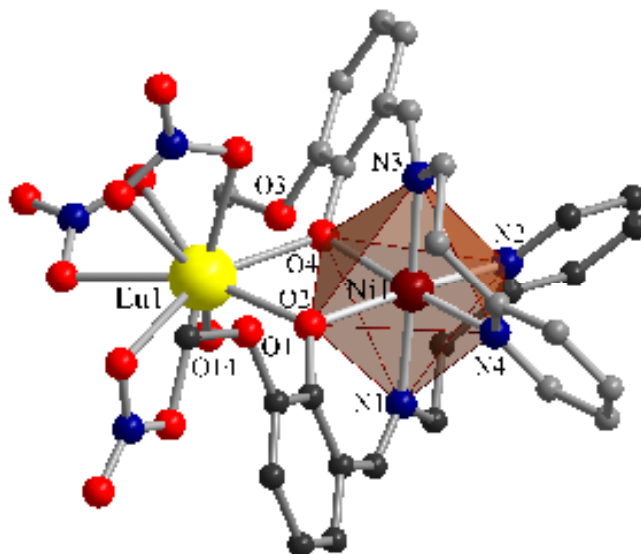
Figure 3.15. Perspective view of [Ni(valaepy)$_2$Eu(O$_2$NO)$_3$(H$_2$O)] in crystal **10**.

Again, as in the case of [Ni(valampy)$_2$Ln] complexes, the two methoxy groups are not coordinated to the europium ion. This is because of the stereochemical requirements of nickel(II) ion, that is, its strong preference for the octahedral geometry orients the two valaepy molecules such that the two methoxy groups are rendered too far from the europium ion to be coordinated.The intermetallic Ni···Eu separation is equal to 3.4898 Å [Ni1 – Eu1 = 3.4898(3) Å].

At the supramolecular level, the dinuclear units interact through hydrogen bonding interactions resulting in the formation of a supramolecular dimer of dinuclear units. The hydrogen bonds are established between the oxygen atom (O14w) of coordinated water of one dinuclear unit and the oxygen atom (O5) of one of the nitrato ligands attached to the europium ion of the neighbouring dinuclear unit, thereby resulting in the formation of double H-bonding bridge [O14w' ··· O5 = 2.77 Å; ' = -*x*, -*y*, 1-*z*] between the two dinuclear units and thus giving rise to a supramolecular dimer of dinuclear units.
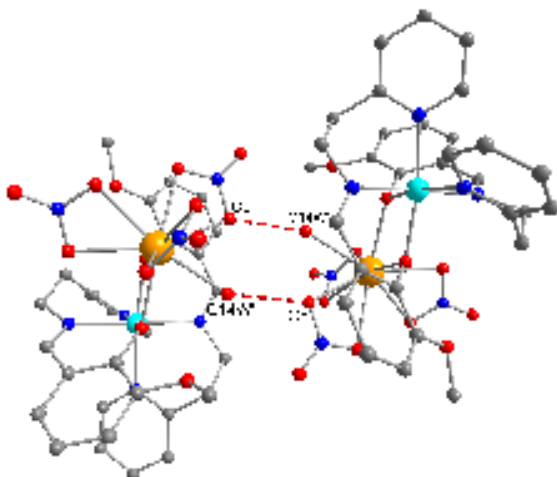
Figure 3.17. Packing diagram of **10** showing the formation of a supramolecular dimer of dinuclear units through the establishment of hydrogen bonding interactions (' = -*x*, -*y*, 1-*z*).

3.3.2. Spectral characterization of heterodinuclear [Ni^{II}(valaepy)$_2$Ln^{III}] Complexes

The heterodinuclear [Ni(valaepy)$_2$Ln^{III}] complexes have been spectroscopically characterized. The IR data of the heterodinuclear [Ni(valaepy)$_2$Ln^{III}] complexes show the presence of the characteristic bands of the organic ligand, nitrato groups attached to the lanthanide ion, as well as the coordinated water molecule.

The UV-Vis-NIR spectra of [Ni^{II}(valaepy)$_2$Ln^{III}] complexes have been recorded in the 200–1300 nm range. For example, the UV-Vis-NIR spectrum of [Ni(valaepy)$_2$Eu(O$_2$NO)$_3$(H$_2$O)]·CH$_3$CN **10**, has been characterized by the presence of a strong absorption band which is assignable to the π–π* transitions of the organic ligand. The characteristic f–f transitions of Eu^{III} ion are not observable in the spectrum because they occur in the 360–400 nm range, a region of spectrum which is masked by the strong absorption band arising due to the organic ligand. The characteristic d–d transitions of Ni^{II} ion occur at 580 nm [$^3A_{2g} \rightarrow {}^3T_{1g}(F)$] and 930 nm [$^3A_{2g} \rightarrow {}^3T_{2g}$]. The shoulder at 430 nm can be attributed to the presence of highest energy $^3A_{2g} \rightarrow {}^3T_{1g}(P)$ transition of Ni^{II} ion.

3.3.3. Magnetic Properties of [Ni^{II}(valaepy)$_2$Ln^{III}] Complexes

The magnetic properties of the heterodinuclear [Ni^{II}(valaepy)$_2$Ln^{III}] family of complexes have also been investigated. In the gadolinium derivative, **11**, ferromagnetic interactions operate between the Ni^{II} and Gd^{III} magnetic centers, while for lanthanide complexes other than gadolinium it is not possible to determine exactly the nature of magnetic exchange interaction because of the intervening first order angular momentum and the crystal field effects of the lanthanide ion. In the case of europium derivative **10**, the decrease of $\chi_M T$ value in the low temperature region can be attributed to the ZFS of Ni^{II} ion, as the Eu^{III} ion is diamagnetic at low temperatures. While the holmium derivative, **13**, clearly shows that ferromagnetic interactions operate between Ni^{II} and Ho^{III} ions in the low temperature range.
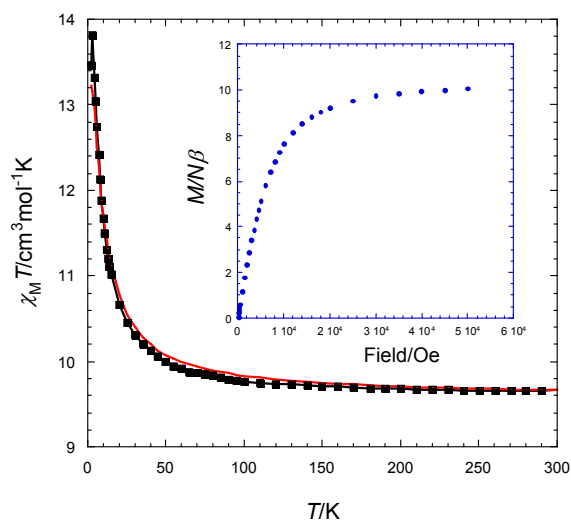
Figure 3.24. $\chi_M T$ curve for [Ni(valaepy)$_2$Gd(O$_2$NO)$_3$(H$_2$O)]·CH$_3$CN **11**. The red solid line represents the best fit to the data.

4. Chapter 4. Heterodinuclear [Cu^{II}Ln^{III}] Complexes with Magnetic Properties

Chapter 4 describes a family of heterodinuclear [Cu^{II}Ln^{III}] complexes, which have been synthesized by using a tetradentate non-compartmental Schiff-base ligand obtained by 1:1 *in-situ* condensation reaction of *o*-vanillin and 2-(2-aminoethyl)-pyridine in acetonitrile solvent.

4.1. Synthetic Strategy

The reaction of stoichiometric amounts of *o*-vanillin (2 mmol) and 2-(2-aminoethyl)-pyridine (2 mmol), in acetonitrile solvent, with $Cu(NO_3)_2 \cdot 3H_2O$ (1 mmol) and $Ln(NO_3)_3 \cdot nH_2O$ (Ln^{III} = Eu, n = 5; Gd, n = 6) (1 mmol) in the presence of triethyl amine, (Et_3N) (4.8 mmol) resulted in the formation of desired products, as shown in Scheme 4.1.
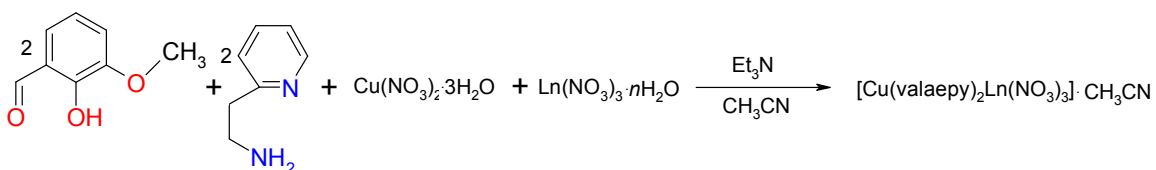
Scheme 4.1. Synthesis of heterodinuclear [Cu^{II}(valaepy)$_2$Ln^{III}] complexes.

4.2.   The [Cu^{II}(valaepy)$_2$Ln^{III}] Family of Heterodinuclear Complexes

The X-ray crystallographic analysis shows that all the heterodinuclear [Cu^{II}(valaepy)$_2$Ln^{III}] complexes are neutral isostructural dinuclear species of general formula [Cu^{II}(valaepy)$_2$Ln^{III}(O$_2$NO)$_3$]·CH$_3$CN (Ln^{III} = Eu **14**, Gd **15**) and crystallize in the monoclinic P*21*/a space group.

4.2.1. Crystallographic Measurements and Structure Description

The crystallographic analysis reveals that in all [Cu^{II}(valaepy)$_2$Ln^{III}] complexes, the Cu(II) ion is pentacoordinated and adopts a trigonal-bipyramidal coordination geometry, being surrounded by two phenoxo oxygen atoms and three nitrogen atoms arising from two Schiff-base ligand moieties, [L^2]$^-$ (valaepy) with one nitrogen atom from a Schiff-base ligand moiety remaining uncoordinated. The lanthanide ion exhibits a coordination number of nine, being surrounded by one methoxy oxygen atom in addition to two bridging phenoxo oxygen atoms arising from Schiff-base ligand moieties, and six oxygen atoms which arise from three chelating bidentate nitrato ligands. The other methoxy oxygen atom remains uncoordinated.

The coordination of methoxy oxygen atoms to the lanthanide ion in the case of heterodinuclear [$Cu^{II}Ln^{III}$] complexes gives rise to a structural type which is different from the hetrodinuclear [$Ni^{II}Ln^{III}$] complexes, in which the methoxy groups are rendered too far to be coordinated because of the stereochemical preference of Ni(II) to adopt a perfect octahedral geometry. This observation underlines the fact that the final architecture of the binuclear complexes is determined by the stereochemical preference of the 3d metal ion.

Figure 4.2. View of the molecular structure of [Cu(valaepy)$_2$Eu(O$_2$NO)$_3$] in crystal in **14**.

4.2.2. Spectral characterization of heterodinuclear [Cu^{II}(valaepy)$_2$Ln^{III}] complexes

The spectroscopic properties of the binuclear [$Cu^{II}Ln^{III}$] complexes have been studied. The IR spectra of [$Cu^{II}Ln^{III}$] complexes exhibit the characteristic bands arising from the chelating nitrato anions coordinated to the lanthanide ion as well important bands due to the Schiff-base ligand moieties.

The electronic spectra of complexes are in accordance with the trigonal-bipyramidal coordination geometry adopted by the Cu(II) ion and also exhibit the characteristic bands of the organic ligands.

Figure 4.7. The electronic spectrum of [Cu(valaepy)$_2$Gd(O$_2$NO)$_3$]·CH$_3$CN **15**.

4.2.3. Magnetic Properties of [Cu^{II}(valaepy)$_2$Ln^{III}] Complexes

The heterodinuclear [Cu^{II}Ln^{III}] complexes exhibit interesting magnetic properties. The gadolinium derivative **15**, exhibits ferromagnetic interaction between Cu^{II} and Gd^{III} ions in accordance with the previously observed phenomenon of ferromagnetic interaction in the heterodinuclear [Cu^{II}Gd^{III}] complexes with similar ligands.
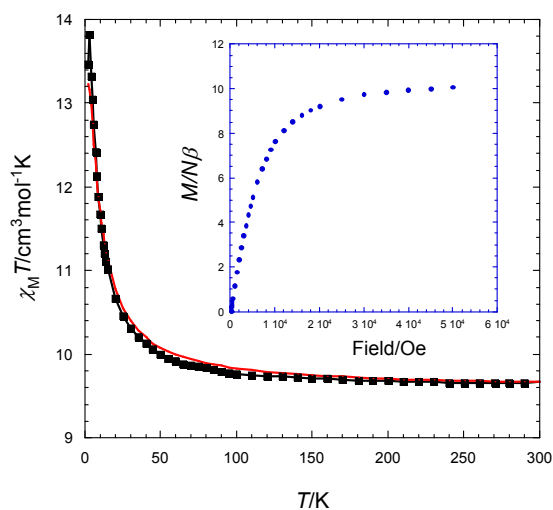
Figure 4.8. Temperature dependence of $\chi_M T$ for [Cu(valaepy)$_2$Gd(O$_2$NO)$_3$]·CH$_3$CN **15**

5. Chapter 5. Heteronuclear [Fe^{III}Ln^{III}] Complexes

Chapter 5 deals with the synthesis, crystallographic investigation, spectroscopic and magnetic characterization of two mononuclear Fe(III) complexes, a tetranuclear [Fe(III)Gd(III)]$_2$ complex and a dinuclear Fe(III) complex, bridged by the dianion of trimesic acid.

5.1. Synthetic Strategy

The mononuclear Fe(III) complex, [Fe(3-MeOsalpn))Cl(H$_2$O)] **16** (where 3-MeOsalpn is a Schiff-base ligand obtained by a condensation reaction of *o*-vanillin and 1,3-diamino-propane in a 2:1 molar ratio) has been synthesized in one pot reaction by mixing stoichiometric amounts of 3-methoxysalicylaldehyde, 1,3-propanediamine and iron(III) chloride in acetonitrile.

1,3-diamino-propane   *o*-vanillin
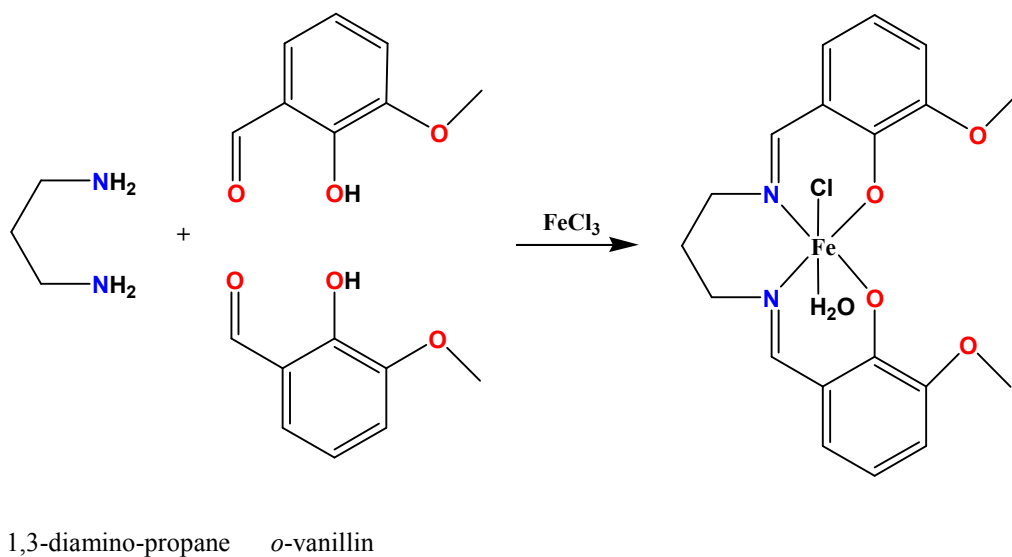
Scheme 5.2. Synthesis of mononuclear Fe(III) complex [Fe(3-MeOsalpn))Cl(H$_2$O)] **16**.

The reaction of mononuclear Fe(III) complex [Fe(3-MeOsalpn))Cl(H$_2$O)] **16** with NH$_4$SCN in a 1:1 molar ratio yielded the complex of formula [Fe(3-MeOsalpn)(NCS)(H$_2$O)]·0.5CH$_3$CN **17**, in which the chloro ligand in **16** is replaced by the thiocyanate ligand.
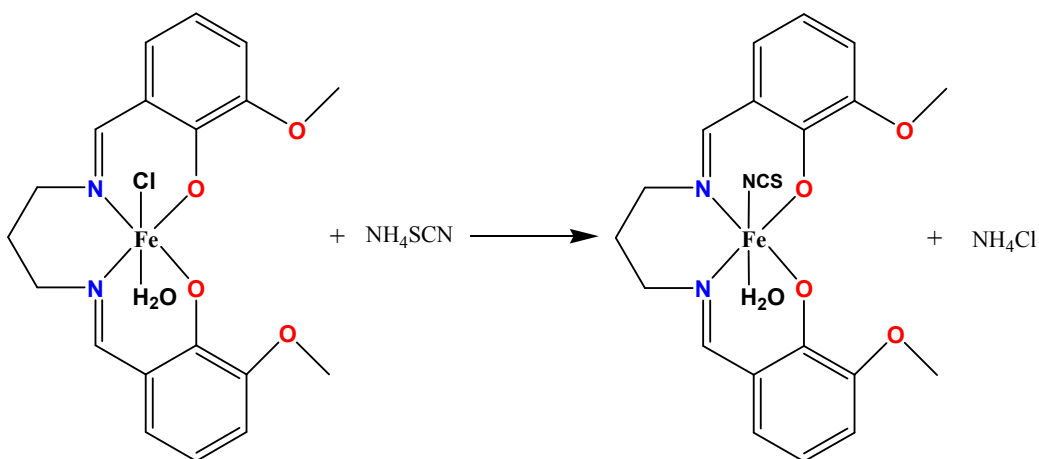
Scheme 5.3. Synthesis of mononuclear Fe(III) complex [Fe(3-MeOsalpn)(NCS)(H$_2$O)]·0.5CH$_3$CN **17**.

Similarly by using mononuclear complex [Fe(3-MeOsalpn))Cl(H$_2$O)] **16** as a ligand toward hydrated gadolinium nitrate yielded the tetranuclear complex [{Fe(3-MeOsalpn)Gd(NO$_3$)$_3$}$_2$(μ-O)]·CH$_3$CN **18**, this complex formation being accompanied by an hydrolytic reaction which account for the resulting oxo-bridged species.
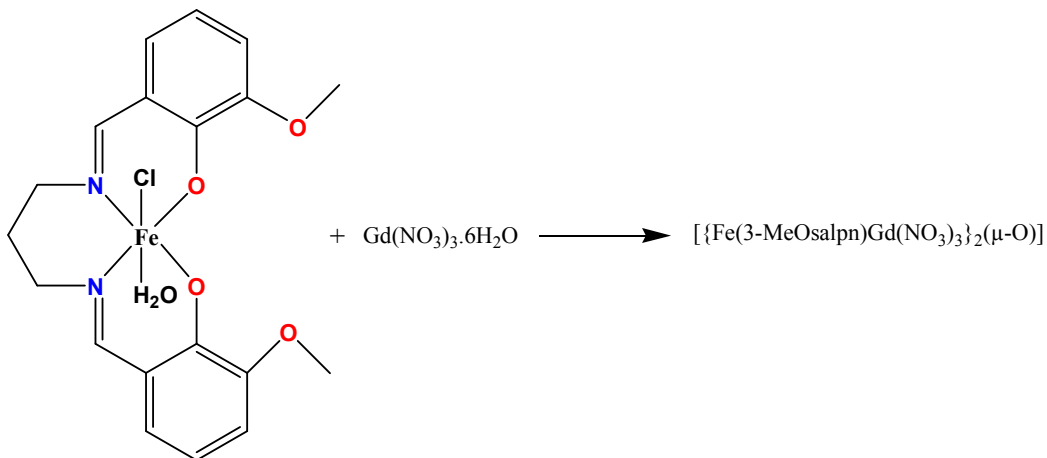
Scheme 5.4. Synthesis of tetranuclear complex [{Fe(3-MeOsalpn)Gd(NO$_3$)$_3$}$_2$(μ-O)]·CH$_3$CN **18**.

The dinuclear iron(III) complex [{Fe(3-MeOsaldmpn)(H$_2$O)}$_2$Htrim]·H$_2$O **19** has been prepared by reacting the mononuclear iron(III) compound [Fe(3-MeOsaldmpn)Cl(H$_2$O)] (where

3-MeOsaldmpn is a Schiff-base ligand obtained by 2:1 condensation reaction of *o*-vanillin and 2,2-dimethyl-1,3-diamino-propane) with trimesic acid in a 2:1 mole ratio.

$+ \; H_3Trim \xrightarrow{\text{LiOH}} [\{Fe(3\text{-MeOsaldmpn})(H_2O)\}_2Htrim].H_2O$
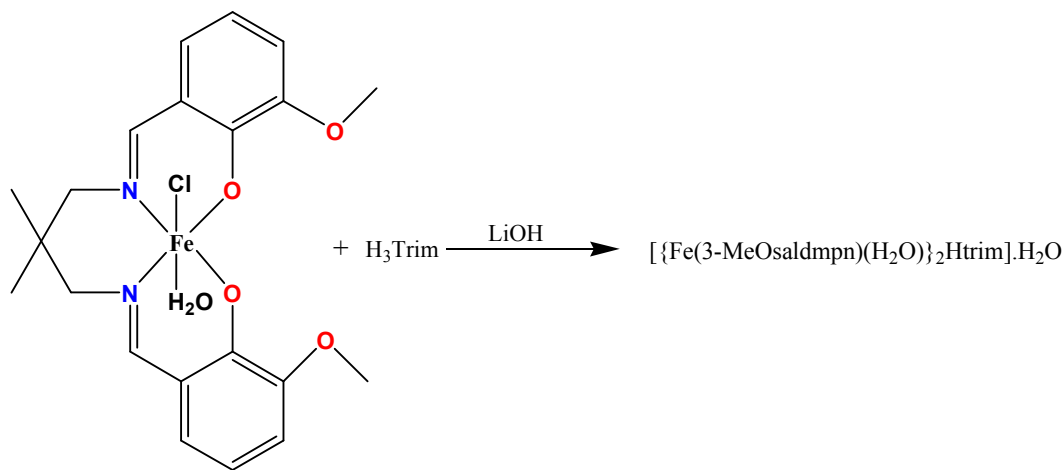
Scheme 5.5. Synthesis of dinuclear Fe(III) complex [{Fe(3-MeOsaldmpn)(H$_2$O)}$_2$Htrim]·H$_2$O **19**.

5.2. Crystallographic Measurements and Structure Description

5.2.1. Description of the Structures of [Fe(3-MeOsalpn)Cl(H$_2$O)] **16**, [Fe(3-MeOsalpn)(NCS)(H$_2$O)]·0.5CH$_3$CN **17** and [{Fe(3-MeOsalpn)Gd(NO$_3$)$_3$}$_2$(μ-O)]·CH$_3$CN **18**.

The Fe(III) ion in mononulear complexes **16** and **17** lies in an octahedral coordination environment in which the basal plane is formed by the tetradentate Schiff-base ligand and the apical positions are occupied by a water molecule and a chloro (**16**) or a thiocyanante (**17**) ligand.

(a)
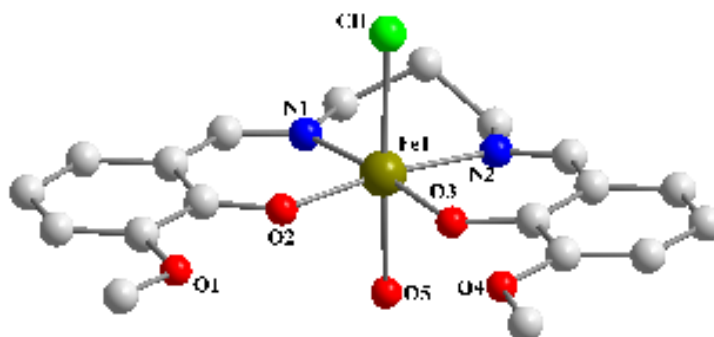
(b)
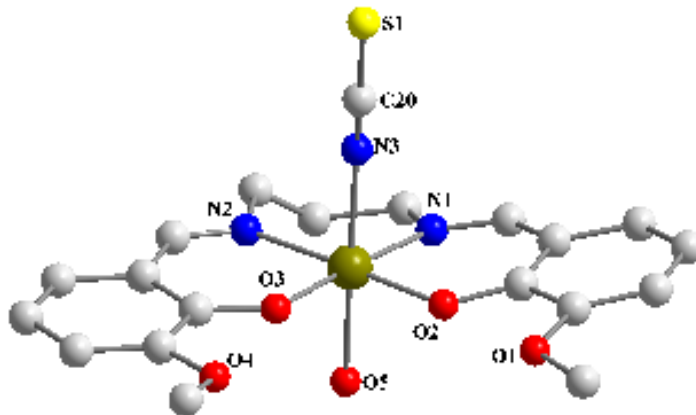
Figure 5.1. Perspective views of: (a) [Fe(3-MeOsalpn)Cl(H$_2$O)] (**16**) and (b) [Fe(3-MeOsalpn)(NCS)(H$_2$O)] (**17**).

The most interesting property of the mononuclear complexes **16** and **17** is the formation of centrosymmetric supramolecular dimers, in which the water molecule coordinated in the apical position of Fe(III) ion is hosted in the open O$_2$O'$_2$ compartment of a neighbouring molecule and forms bifurcated hydrogen bonds. Moreover, the stability of the resulting supramolecular dimers is enhanced by the π–π stacking interactions between the aromatic rings of the Schiff-base (3.4 – 3.6 Å).

(a)
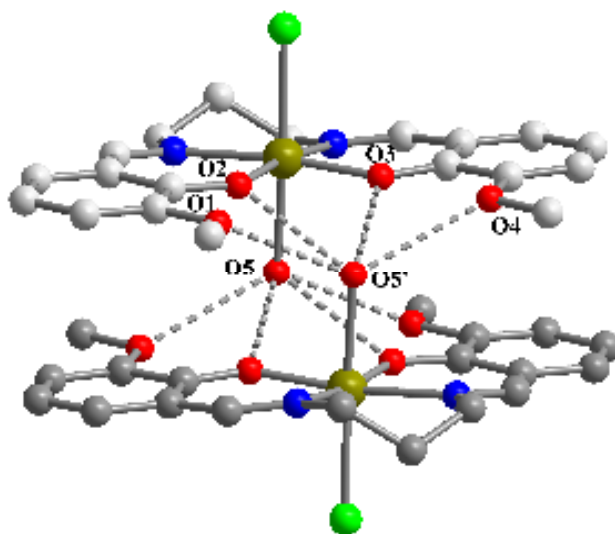
(b)
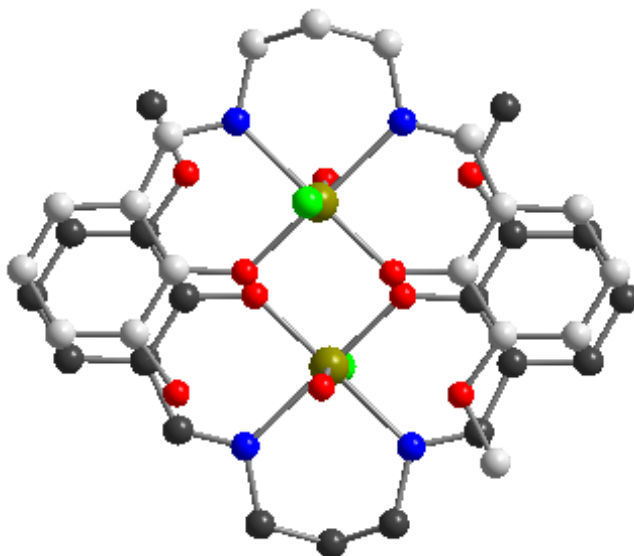
Fig. 5.2. Details of the packing of the neutral complexes in **16**: (a) Formation of the supramolecular dinuclear assembly (symmetry code: (') = 2-*x*,-*y*,1-*z*); (d) $\pi-\pi$ stacking interactions within the supramolecular dimmer.

The crystal structure of [{Fe(3-MeOsalpn)Gd(NO$_3$)$_3$}$_2$(μ-O)]·CH$_3$CN **18** consists of neutral [{Fe(3-MeOsalpn)Gd(NO$_3$)$_3$}$_2$(μ-O)] tetranuclear species, the two {Fe(3-MeOsalpn)Gd(NO$_3$)$_3$} moieties being connected by an oxo bridge established between the

iron(III) ions. Each iron(III) ion in **18** is five-coordinated in a square-pyramidal geometry. The basal plane is formed by two nitrogen atoms and two phenolato oxygens arising from the Schiff-base ligand. The apical position is occupied by the oxo-bridge.
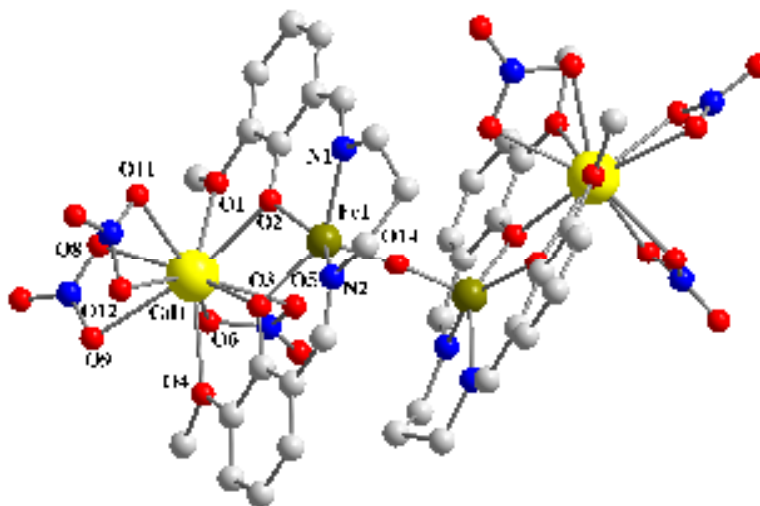
Figure 5.3. Perspective view of [{Fe(3-MeOsalpn)Gd(NO$_3$)$_3$}$_2$(μ-O)] **18**.

5.2.2. Description of the Structure of [{Fe(3-MeOsaldmpn)(H$_2$O)}$_2$Htrim]·H$_2$O **19**

The crystal structure of **19** consists of neutral [{Fe(3-MeOsaldmpn)H$_2$O}$_2$Htrim]·H$_2$O dinuclear species, the two {Fe(3-MeOsaldmpn)(H$_2$O)} moieties being connected by the dianion of the trimesic acid in which the two deprotonated carboxylic groups are coordinated in a monodentate bridging mode onto the axial position of the two iron(III) ions. The third carboxylic group remains protonated giving overall a neutral complex. Each iron(III) in **19** is six-coordinated in a somewhat distorted octahedral coordination mode. The basal plane is formed by two nitrogen atoms and two phenolato oxygens of the Schiff-base. The apical positions are occupied by one water molecule and one oxygen atom from one carboxylato group of the bridging trimesate dianion.
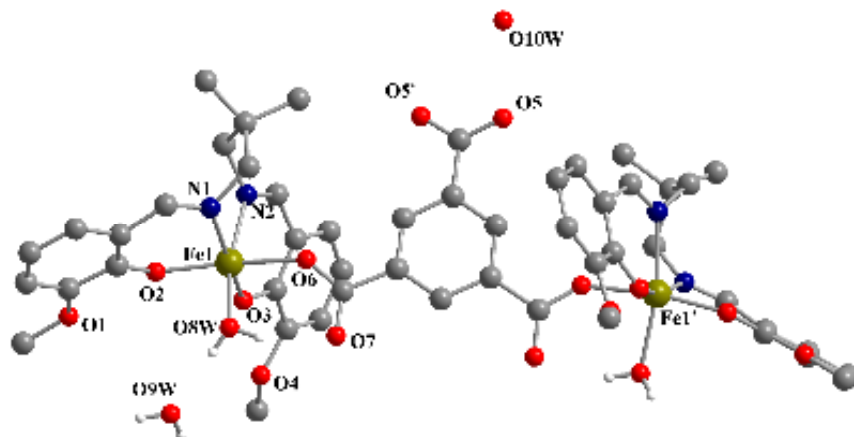
Figure 5.4. Perspective view of [{Fe(3-MeOsaldmpn)H$_2$O}$_2$Htrim]·H$_2$O (**19**).

The crystallization water molecules hosted in the outer O$_2$O'$_2$ compartments of dinuclear Fe(III) complex **19** are involved in the bifurcated hydrogen bonds with the phenoxo and methoxy oxygen atoms. Moreover, these crystallization water molecules hosted in the O$_2$O'$_2$ compartments act as hydrogen bond acceptors for water molecules coordinated to metal ions of the neighbouring complexes generating supramolecular chains.
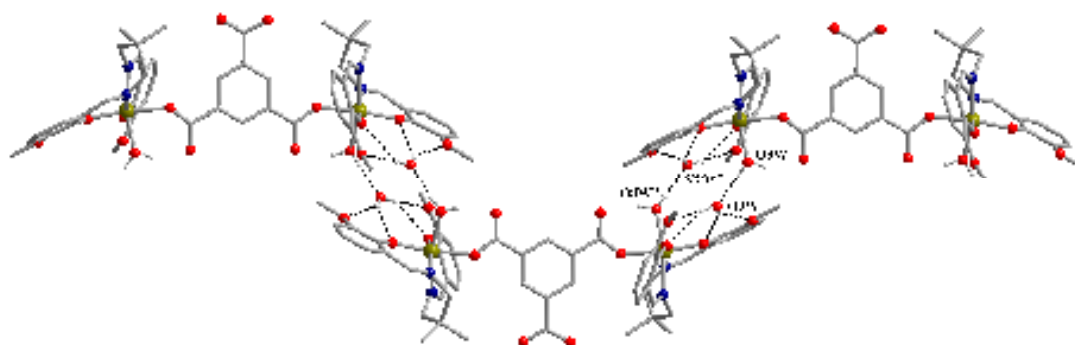
Figure 5.5. Perspective view of the supramolecular chains generated by hydrogen bond interactions in **19**.

5.3. Spectral characterization of Fe(III) mononuclear and polynuclear complexes

The IR spectra of mononuclear Fe(III) complexes [Fe(3-MeOsalpn)Cl(H$_2$O)] **16** and [Fe(3-MeOsalpn)(NCS)(H$_2$O)] **17**, show the presence of bands due to the Schiff-base ligands, coordinated water molecules and thiocyanate ligand (in case of **17**). The important bands in the

IR spectrum of tetranuclear complex [{Fe(3-MeOsalpn)Gd(NO$_3$)$_3$}$_2$(μ-O)]·CH$_3$CN **18**, arise from the presence of coordinated nitrato ions and the oxo-bridge. The dinuclear Fe(III) complex [{Fe(3-MeOsaldmpn)(H$_2$O)}$_2$Htrim]·H$_2$O **19**, shows bands due to the stretching vibrations of the carboxyl groups of the bridging dianion of the trimesic acid as well as water molecules coordinated in the axial position of two iron(III) moieties, and the crystallization water molecule.

The electronic spectra of the mononuclear Fe(III) complexes [Fe(3-MeOsalpn)Cl(H$_2$O)] **16** and [Fe(3-MeOsalpn)(NCS)(H$_2$O)] **17**, exhibit almost similar features with the presence of relatively intense absorption band (λ_{max} = 570 nm) in the visible region which can be attributed to the charge transfer transitions from the p$_\pi$ orbitals of the phenolic oxygens to the d$_\pi$* orbitals of the Fe(III) ion.[24] The charge transfer band partially obscures the absorption band occurring in the UV region which arises due to the intraligand π–π* transitions. The electronic spectra of tetranuclear complex [{Fe(3-MeOsalpn)Gd(NO$_3$)$_3$}$_2$(μ-O)]·CH$_3$CN **18** and dinuclear Fe(III) complex [{Fe(3-MeOsaldmpn)(H$_2$O)}$_2$Htrim]·H$_2$O **19** are characterized by the presence of ligand–metal charge transfer (LMCT) bands and absorption band arising due to the organic ligand. Two strong bands in the UV and visible region of the spectra are the ligand–metal charge transfer (LMCT) bands. The lower energy band corresponds to the transitions from the filled p$_\pi$ orbitals of the phenolate oxygen to the empty d$_\pi$* orbitals of the Fe^{III} metal center, while the higher energy band can be attributed to the transition from the phenolate p$_\pi$ orbitals to Fe^{III} d$_\sigma$* orbital.[27] The absorption band (shoulder) with the maximum (λ_{max}) in the UV region is attributable to the intraligand π–π* transitions.

5.4.   Magnetic Properties of Fe(III) Complexes

The magnetic susceptibilty measurements for the mononuclear Fe(III) complexes **16** and **17** show the presence of weak antiferromagnetic interactions within the supramolecular dinuclear unit. The susceptibility data for the mononuclear Fe(III) complexes **16** and **17** were analysed by full-matrix diagonalization of the following spin Hamiltonian [eq (1)],

$$\boldsymbol{H} = -J\boldsymbol{S}_1 \cdot \boldsymbol{S}_2 + D_1[\boldsymbol{S}_{1z}^2 - 1/3S_1(S_1 + 1)] + D_2[\boldsymbol{S}_{1z}^2 - 1/3S_2(S_2 + 1)] + \beta H(g_1\boldsymbol{S}_1 + g_2\boldsymbol{S}_2) \qquad (1)$$

The first term refers to the isotropic exchange interaction between the iron(III) ions within the supramolecular dimer, the second and the third ones take into account the zero-field splitting (ZFS) effects for the two iron ions ($D_1 = D_2$) and the two last ones account for the Zeeman effects ($g_1 = g_2 = g$). The best fit to the data leads to the following set of parameters: $g = 1.98$; $J = -0.76$ cm^{-1}, $|D| = 0.21$ cm^{-1} for **16** and $g = 1.96$, $J = -0.75$ cm^{-1}, $|D| = 0.0$ cm^{-1} for **17**.
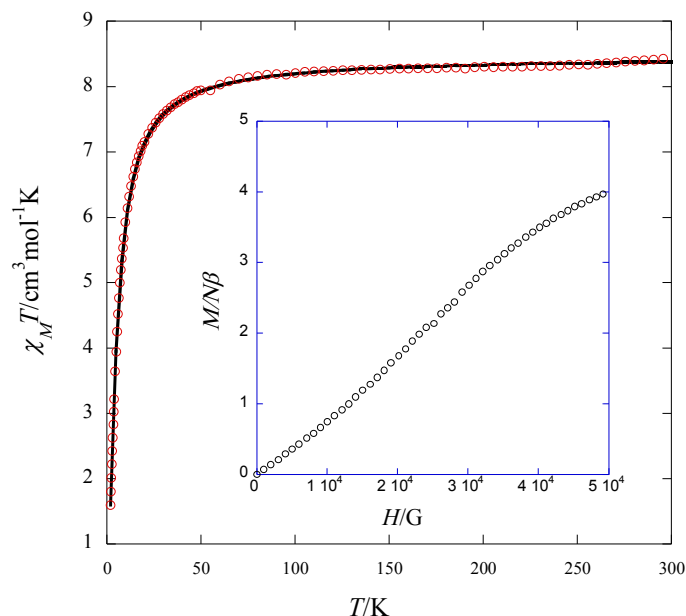
Figure 5.14. The $\chi_M T$ vs. T curve for complex **16**. The solid line represents the best fit to the data. Inset: magnetization vs applied magnetic field curves at 2.0 K.

In the case of tetranuclear complex **18**, antiferromagnetic interactions operate between the oxo-bridged Fe(III) ions. Given the tetranuclear structure of **18**, its magnetic data were analyzed through the isotropic spin Hamiltonian of eq (2)

$$\boldsymbol{H} = -J(\boldsymbol{S}_{Gd1}\boldsymbol{S}_{Fe1} + \boldsymbol{S}_{Fe2}\boldsymbol{S}_{Gd2}) - J'\boldsymbol{S}_{Fe1}\boldsymbol{S}_{Fe2} + \beta H(g_{Fe1}\boldsymbol{S}_{Fe1} + g_{Fe2}\boldsymbol{S}_{Fe2} + g_{Gd1}\boldsymbol{S}_{Gd1} + g_{Gd2}\boldsymbol{S}_{Gd2}) \quad (2)$$

where J and J' are the magnetic coupling through the double phenoxo and single oxo pathways respectively and $g_{Fe} = g_{Gd} = g$ (the average Landé factor). It was assumed that the intramolecular magnetic coupling between the two gadolinium(III) ions is negligible. Best-fit parameters through numerical matrix diagonalization techniques by using a Fortran program[29] are: $J = -3.25$ cm^{-1}, $J' = -275$ cm^{-1} and $g = 2.0$.
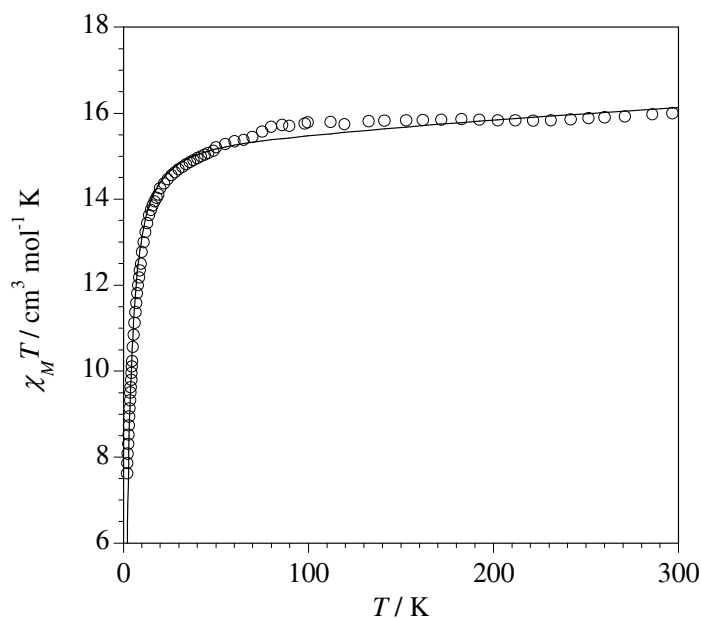
Figure 5.16. The $\chi_M T$ vs. T curve for compound **18**. The solid line represents the best fit to the data.

Similarly in the dinuclear Fe(III) complex **19**, the dianion of trimesic acid transmits weak antiferromagnetic interactions between the two Fe(III) ions. The magnetic data are analyzed by using the isotropic spin Hamiltonian for a simple binuclear complex:

$$H = -J\mathbf{S}_{Fe1}\mathbf{S}_{Fe1'}$$

The best fit to the data leads to the following set of parameters: $g = 1.93$; $J = -0.12$ cm^{-1}.

6. Chapter 6. Hexanuclear Copper(II) Complex With Compartmental Schiff-base Ligand

6.1. Synthesis

Chapter 6 describes the synthesis, crystallographic investigation and spectroscopic properties of a novel hexanuclear Cu(II) complex **20**, which is prepared by one-pot reaction of an end-off bicompartmental Schiff-base ligand, HL^4 (which is obtained by *in-situ* condensation of

2,6-dimethyl-4-methyl-phenol with 1-(2-aminoethyl)-piperazine in a 1:2 molar ratio), with the copper(II) nitrate salt in basic medium.
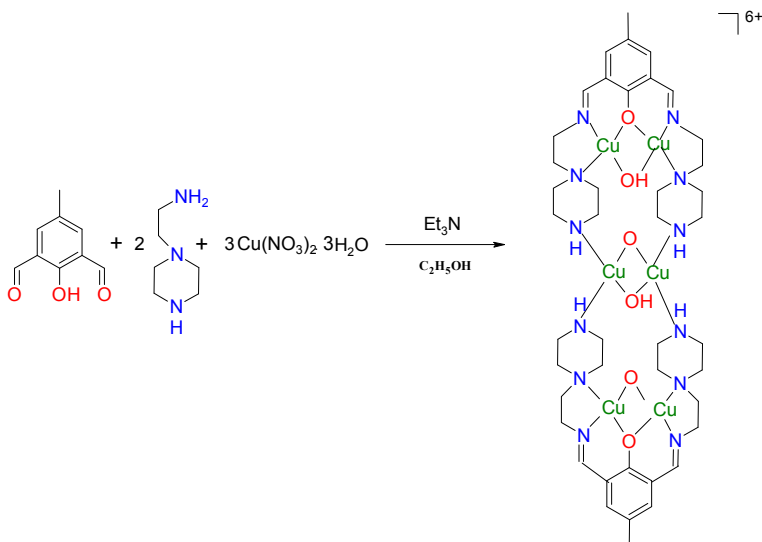
Scheme 6.3. Synthesis of hexanuclear Cu(II) complex **20**.

6.2. Crystallographic Measurements and Structure Description

The X-ray analysis of hexanuclear Cu(II) complex **20** shows that the asymmetric unit is composed of two crystallographically independent molecules **A** and **B**. The units **A** and **B** exhibit a fascinating structure in which the two binuclear cationic moieties are interconnected with each other by two more copper(II) ions through the tertiary nitrogen atoms of diamine functionality of Schiff-base ligands. These two copper(II) ions are also interconnected with each other through double hydroxo bridge. The diamine functionality of bicompartmental Schiff-base ligands adopts a chair conformation, to facilitate the coordination of tertiary nitrogen atoms with the copper(II) ions.

(A)   (B)
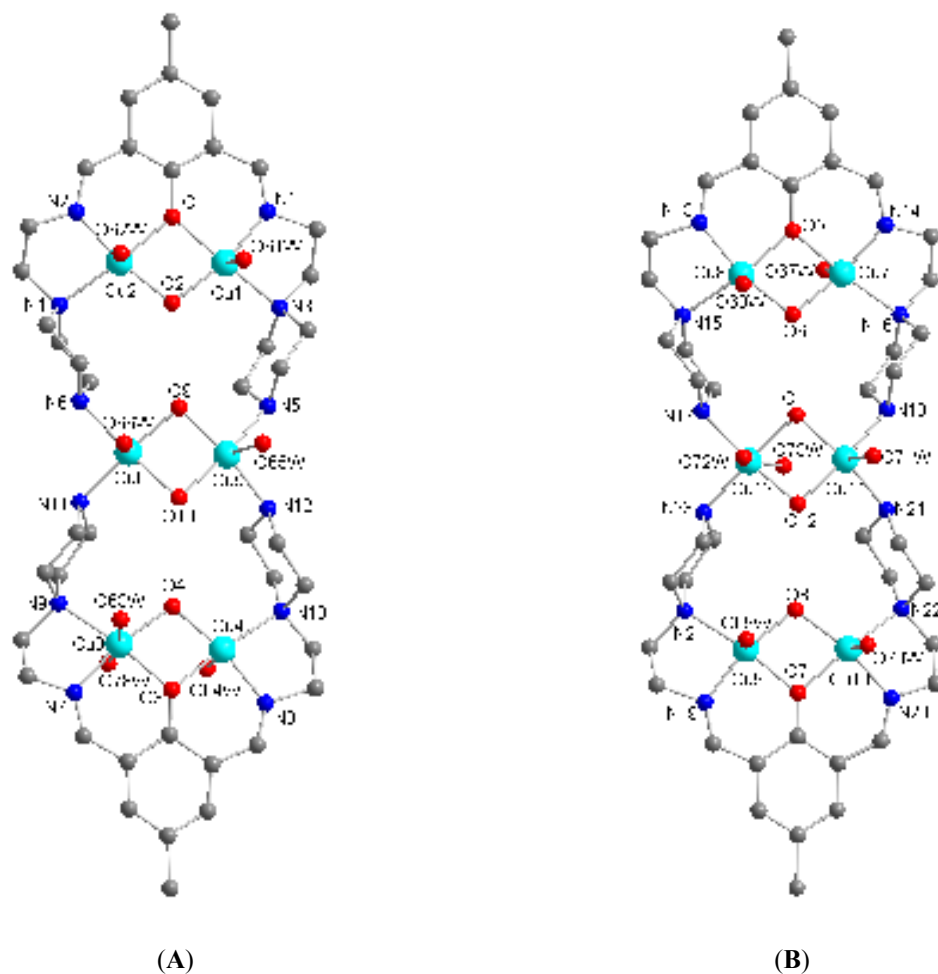
Figure 6.2. Molecular structures of two independent units (**A** and **B**) in assymetric unit of Cu(II) hexanuclear complex, **20**.

6.3.   Spectral characterization of hexanuclear Cu(II) complex 20

The complex **20** has been spectroscopically characterized, the IR spectrum showing the presence of uncoordinated nitrato ions which act as counter ions and the bridging hydroxo groups.

The electronic absorption spectrum of **20** shows bands arising due to the d–d transitions of Cu(II) ions, situated in the square-pyramidal coordination geometry as well as bands due to the intraligand π–π* transitions of the Schiff-base ligand and charge transfer transitions.
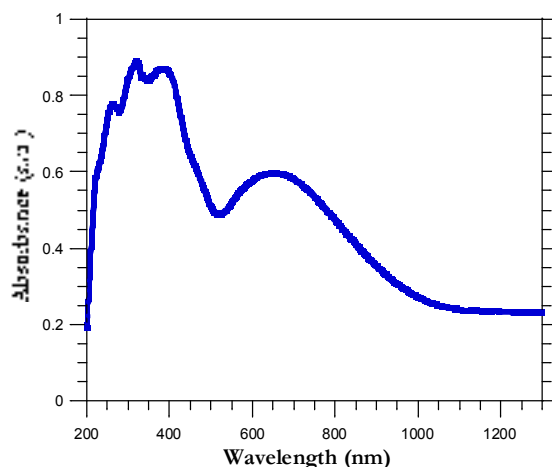
Figure 6.4. The electronic spectrum of Cu(II) hexanuclear complex, **20**.

CONCLUSIONS

In conclusion **20** new complexes have been isolated as single-crystals and subsequently characterized through X-ray diffraction measurements. Spectroscopic (IR, UV-Vis-NIR, excitation and emission spectra) and magnetic measurements have also been employed in order to characterize the novel compounds, revealing interesting molecular, solid-state architectures and useful properties.

All of the new complexes have discrete structures, ranging from mononuclear complexes (**16**, **17**) to dinuclear (**1−15**, **19**), tetranuclear (**18**) or hexnuclear (**20**) species. Compounds **1−6** are [$Zn^{II}Ln^{III}$] binuclear complexes, **7-13** are [$Ni^{II}Ln^{III}$] binuclear complexes, and **14−15** are [$Cu^{II}Ln^{III}$] binuclear complexes. The complexes **16** and **17** are mononuclear Fe^{III} compounds, **18** is a tetranuclear [$Fe^{III}Gd^{III}$]$_2$ compound and complex **19** is a dinuclear Fe^{III} compound. Compound **20** is a hexanuclear copper(II) complex.

Selected References

[24]   (a) E. W. Ainscough, A.M. Brodie, J. E. Plowman, K. L. Brown, A. W. Addison, A. R. Gainsford, *Inorg. Chem.* **1980**, *19*, 3655; (b) B. P. Gaber, V. Miskowski, T. G. Spiro, *J.*

Am. Chem. Soc. **1974**, *96*, 6868; (c) C. Flassbeck, K. Wieghardt, *Z. Anorg. Allg. Chem.* **1992**, *608*, 60.

[25] J. C. G. Bunzli, G. R. Chopin, In *Lanthanide Probes in Life, Chemical, and Earth Sciences: Theory and Practice*; Elsevier: Amsterdam, **1989**.

[27] C. A. Brown, G. J. Rennar, R. L. Musselman, E. I. Solomon, *Inorg. Chem.* **1995**, *34*, 688.

[28] (a) J.-P. Costes, F. Dahan, A. Dupuis and J.-P. Laurent, *Inorg. Chem.* **1996**, *35*, 2400; (*b*) M. Sakamoto, K. Manseki and H. Okawa, *Coord. Chem. Rev.* **2001**, *219–221*, 379; (*c*) A. J. Atkins, D. Black, A. J. Blake, A. Marin-Becerra, S. Parsons, L. Ruiz-Ramirez and M. Schröder, *Chem. Commun.* **1996**, 457; (*d*) H. Okawa, H. Furutachi and D. E. Fenton, *Coord. Chem. Rev.* **1998**, *174*, 51; (e) R. Gheorghe, P. Cucos, M. Andruh, J.-P. Costes, B. Donnadieu and S. Shova, *Chem.–Eur. J.* **2006**, *12*, 187.

[29] J. Cano, *VMPAG package*, University of València, Spain, **2003**.

[108] M. Sarwar, A. M. Madalan, C. Tiseanu, G. Novitchi, C. Maxim, G. Marinescu, D. Luneau, M. Andruh, manuscript in preparation.

[109] M. Sarwar, A. M. Madalan, F. Lloret, M. Julve, M. Andruh, *Polyhedron* **2011**, *30*, 2414.

[110] M. Sarwar, A. M. Madalan, C. Maxim, M. Andruh, *Rev. Roum. de Chemie*, accepted for publication.

Papers in International Journals

The original results of this thesis have been the subject of three papers: Two papers have already been published (1-2), and the manuscript for the third paper has been submitted to Journal Dalton Transactions (3):

[1] **M. Sarwar**, A. M. Madalan, F. Lloret, M. Julve, M. Andruh, "Mononuclear Fe(III) and Tetranuclear [Fe(III)Gd(III)]$_2$ Complexes with a Schiff-Base Ligand Derived from the *o*-

Vanillin: Synthesis, Crystal Structures and Magnetic Properties", *Polyhedron* **2011**, *30*, 2414-2420.

[2]   **M. Sarwar**, A. M. Madalan, C. Maxim, M. Andruh, "A Dinuclear Iron(III) Complex Bridged by the Dianion of Trimesic Acid – [{Fe(3-MeOsaldmpn)(H$_2$O)}$_2$Htrim]·H$_2$O: Synthesis, Crystal Structure and Magnetic Properties", *Rev. Roum. Chim.* **2012**, *57*(*7-8*), 687-691.

[3]   **M. Sarwar**, A. M. Madalan, C. Tiseanu, G. Novitchi, C. Maxim, G. Marinescu, D. Luneau, M. Andruh, "A new synthetic route towards binuclear 3d-4f complexes, using non-compartmental ligands derived from *o*-vanillin. Syntheses, crystal structures, magnetic and luminescent properties" – Manuscript submitted to Journal *Dalton Transactions*.

Participations at International Chemistry Conferences

The original results presented in this thesis have been the subject of two oral presentations (1-2) and a poster presentation (3) at International Chemistry Conferences.

[1]   **M. Sarwar**, A. M. Madalan, M. Andruh, "Mononuclear Iron(III) Schiff-base Complexes as Precursors in Crystal Engineering", *The 31st Romanian National Chemistry Conference*, Ramnicu Valcea, Romania, 2010.

[2]   **M. Sarwar**, A. M. Madalan, M. Andruh, "Synthesis and Characterization of 3d-4f Binuclear Complexes by Using Compartmental Schiff-base ligands", *The 32nd Romanian National Chemistry Conference*, Ramnicu Valcea, Romania, 2012.

[3]   **M. Sarwar**, A. M. Madalan, M. Andruh, "3d-4f Binuclear Complexes: Synthesis, Crystal Structures, Magnetic and Luminescence Properties", *New Trends in Materials Science workshop*, Romanian Academy, Bucharest, Romania, 2012.

Participations at Students' Scientific Communications Sessions

The original results presented in this PhD thesis have been the subject of two oral presentations at the Students' Scientific Communications Sessions.

[1]   **M. Sarwar**, A. M. Madalan, M. Andruh, "Mononuclear Fe(III) and tetranuclear [Fe(III)Gd(III)]$_2$ complexes with a Schiff-base ligand derived from the *o*-vanillin: Synthesis, crystal structures and magnetic properties", *Student Scientific Communications Session*, Faculty of Chemistry, University of Bucharest, Romania, 2011.

[2]   **M. Sarwar**, A. M. Madalan, M. Andruh, "Synthesis and Characterization of Heteropolynuclear Complexes by Using Compartmental Schiff-base Ligands", *Student Scientific Communications Session*, Faculty of Chemistry, University of Bucharest, Romania, 2012.